CHEMISTRY
A EUROPEAN JOURNAL

DOI: 10.1002/chem.200700534

Homoleptic Rare-Earth Metal(III) Tetramethylaluminates: Structural Chemistry, Reactivity, and Performance in Isoprene Polymerization

Melanie Zimmermann,[a] Nils Åge Frøystein,[a] Andreas Fischbach,[b] Peter Sirsch,[c] H. Martin Dietrich,[a] Karl W. Törnroos,[a] Eberhardt Herdtweck,[d] and Reiner Anwander*[a]

Abstract: The complexes $[Ln(AlMe_4)_3]$ (Ln = Y, La, Ce, Pr, Nd, Sm, Ho, Lu) have been synthesized by an amide elimination route and the structures of $[Lu\{(\mu\text{-}Me)_2AlMe_2\}_3]$, $[Sm\{(\mu\text{-}Me)_2AlMe_2\}_3]$, $[Pr\{(\mu\text{-}Me)_2AlMe_2\}_3]$, and $[La\{(\mu\text{-}Me)_2AlMe_2\}_2\{(\mu\text{-}Me)_3AlMe\}]$ determined by X-ray crystallography. These structures reveal a distinct Ln^{3+} cation size-dependency. A comprehensive insight into the intrinsic properties and solution coordination phenomena of $[Ln(AlMe_4)_3]$ complexes has been gained from extended dynamic ^1H and ^{13}C NMR spectroscopic studies, as well as 1D ^{89}Y, 2D $^1H/^{89}Y$, and ^{27}Al NMR spectroscopic investigations. $[Ce(AlMe_4)_3]$ and $[Pr(AlMe_4)_3]$ have been used as alkyl precursors for the synthesis of heterobimetallic alkylated rare-earth metal complexes. Both carboxylate and siloxide ligands can be introduced by methane elimination reactions that give the heterobimetallic complexes $[Ln\{(O_2CAr^{iPr})_2(\mu\text{-}AlMe_2)\}_2(AlMe_4)(C_6H_{14})_n]$ and $[Ln\{OSi(OtBu)_3\}(AlMe_3)(AlMe_4)_2]$, respectively. $[Pr\{OSi(OtBu)_3\}(AlMe_3)(AlMe_4)_2]$ has been characterized by X-ray structure analysis. All of the cerium and praseodymium complexes are used as precatalysts in the stereospecific polymerization of isoprene (1–3 equivalents of Et_2AlCl as co-catalyst) and compared to the corresponding neodymium-based initiators reported previously. The superior catalytic performance of the homoleptic complexes leads to quantitative yields of high-*cis*-1,4-polyisoprene (>98%) in almost all of the polymerization experiments. In the case of the binary catalyst mixtures derived from carboxylate or siloxide precatalysts quantitative formation of polyisoprene is only observed for $n_{Ln}:n_{Cl}=1:2$. The influence of the metal size is illustrated for the heterobimetallic lanthanum, cerium, praseodymium, neodymium, and gadolinium carboxylate complexes, and the highest activities are observed for praseodymium as a metal center in the presence of one equivalent of Et_2AlCl.

Keywords: aluminum · homogeneous catalysis · lanthanides · NMR spectroscopy · polymerization

Introduction

Since the first successful isolation of organometallic derivatives of the rare-earth elements (Ln),[1] the synthesis of homoleptic alkyl complexes (LnR_3) has posed a continual challenge in the field of experimental organolanthanide chemistry.[2–4] Simple alkyl ligands such as methyl and ethyl have been found to be incapable of coping with the stereoelectronic demands of the large and highly oxophilic Ln^{3+} metal centers, and it was not until the late 1980s that donor-free LnR_3 compounds containing very bulky alkyl ligands ($R=CH(SiMe_3)_2$) were isolated and characterized.[5] Donor (D)-solvated alkyl derivatives $[LnR_3(D)_n]$ are routinely used as precursor compounds for the synthesis of heteroleptic derivatives $[L_xLnR_y(D)_m]$ $(x+y=3)$ that provide an efficient entry into organolanthanide-based catalysis as well as unique model systems for studying elementary processes in

[a] M. Zimmermann, Dr. N. Å. Frøystein, Dr. H. M. Dietrich, Prof. Dr. K. W. Törnroos, Prof. Dr. R. Anwander
Department of Chemistry, University of Bergen
Allégaten 41, 5007 Bergen (Norway)
Fax: (+47) 555-89-490
E-mail: reiner.anwander@kj.uib.no

[b] Dr. A. Fischbach
Current address: OXEA Deutschland GmbH
Otto-Roelen-Strasse 3, 46147 Oberhausen (Germany)

[c] Dr. P. Sirsch
Department of Chemistry, University of New Brunswick
Fredericton, NB E3B 6E2 (Canada)

[d] Dr. E. Herdtweck
Department Chemie, Lehrstuhl für Anorganische Chemie
Technische Universität München
Lichtenbergstrasse 4, 85747 Garching bei München (Germany)

olefin polymerization.[4] However, their implementation in this area has been hampered by several factors. Thus, besides the formation of polymeric network structures,[6] "ate" complexes,[7] and the need for stabilizing donor molecules,[8–11] the availability and stability of rare-earth metal alkyl precursors is very much dependent on the size of the Ln^{3+} ion. To date, $[LnMe_3]_x$ (Ln = Y, Ho, Lu),[6] $[Ln(CH_2SiMe_3)_3(thf)_x]$ (Ln = Sc, Y, Er, Yb, Lu, $x = 2$; Ln = Y, Sm, $x = 3$),[8] $[Ln(CH_2SiMe_2Ph)_3(thf)_2]$ (Ln = Sc, Y),[9] $[Ln(CH_2tBu)_3(thf)_2]$ (Ln = Sc, Y, Yb),[8a,10] $[La(CH_2Ph)_3(thf)_3]$, $[La(CH_2Ph\text{-}4\text{-}Me)_3(thf)_3]$,[11] $[La\{CH(PPh_2)_2\}_3]$,[12] $[Ln(o\text{-}Me_2NC_6H_4CH_2)_3]$ (Ln = Sc, Y, La, Lu),[13] and $[Ln\{CH(SiMe_3)_2\}_3]$ (Ln = Y, La, Nd, Sm, Lu)[5] are the only fully characterized rare-earth metal tris(alkyl) complexes. Their suitability for alkane-elimination reactions, however, is affected by the low stability and unavailability of the envisaged large or small Ln^{3+} ion in many cases.

Homoleptic tris(tetramethylaluminate) complexes $[Ln(AlMe_4)_3]$ found entry into organolanthanide synthesis only recently, some 10 years after their discovery.[14,15] Their straightforward high-yield synthesis and their availability for the entire Ln^{3+} size-range, except scandium, without ate complex formation make these "metal alkyls in disguise" versatile synthetic precursors for the generation of a variety of heterobimetallic Ln/Al complexes.[16,17] Recent publications in this field have emphasized the suitability of $[Ln(AlMe_4)_3]$ complexes for both the synthesis of half-lanthanidocene[18] and lanthanidocene complexes[19] and also post-lanthanidocene derivatives.[20,21] Thus, $[Ln(AlMe_4)_3]$ complexes can undergo protonolysis reactions—$[AlMe_4]\rightarrow$[ligand-H] exchange—that lead to the formation of methane and trimethylaluminum as the only by-products,[16,18] as well as salt-metathesis reactions involving $[AlMe_4^-]\rightarrow[ligand^-]$ exchange.[22] The formation of distinct heteroleptic tetramethylaluminate complexes depending on the Ln^{3+} size[20,21] has been ascribed to different reaction pathways arising from attack at either the bridging or terminal methyl groups of a Ln-bonded $[AlMe_4^-]$ ligand, therefore comprehensive insight into the intrinsic properties and solution/solid-state coordination phenomena of $[Ln(AlMe_4)_3]$ complexes seems to be crucial for understanding their enhanced reactivity, be it in alkane elimination,[23,24] methyl group transfer (alkylation) reactions,[21] or catalytic diene polymerization.[17]

Herein, we would like to discuss a detailed study of homoleptic rare-earth metal tris(tetramethylaluminate) complexes that involves varying the synthetic approach, several X-ray structure analyses, and dynamic and heteronuclear NMR spectroscopy. Furthermore, $[Ln(AlMe_4)_3]$ complexes have been used as alkyl precursors for the synthesis of rare-metal metal carboxylate and siloxide tetramethylaluminate complexes and their catalytic performance as binary isoprene polymerization catalysts has been investigated.

Results and Discussion

Synthesis of Ln^{3+} tetramethylaluminate complexes: The general synthesis of homoleptic $[Ln(AlMe_4)_3]$ complexes, first reported for the metals yttrium, neodymium, and samarium in 1995 (Scheme 1),[14,17] gave the trimethylaluminum

$$[LnCl_3(thf)_x] + 3\ LiNMe_2 \xrightarrow[RT,\ 18h]{THF} [Ln(NMe_2)_3(LiCl)_3]$$

$$[Ln(NMe_2)_3(LiCl)_3] + 6\ AlMe_3 \xrightarrow[RT,\ 18h]{hexane} [Ln(AlMe_4)_3] + 1.5\ [\{Me_2AlNMe_2\}_2] + 3\ LiCl$$

Scheme 1. Synthesis of homoleptic rare-metal metal(III) tetramethylaluminates (Ln = Y (**1a**), La (**1b**), Nd (**1e**), Sm (**1f**), Ho (**1g**), and Lu (**1h**)).

inclusion products $[Ln(AlMe_4)_3(Al_2Me_6)_{0.5}]$. The Ln^{3+} tetramethylaluminate complexes of Y (**1a**), La (**1b**), Nd (**1e**), Sm (**1f**), Ho (**1g**), and Lu (**1h**) were obtained in good overall yields by following this original procedure. Several crystallization steps were necessary to obtain crystalline, trimethylaluminum-free $Ln(AlMe_4)_3$ complexes, with the actual number of steps depending on the size of the Ln^{3+} ion (Lu $\gg$ Y, Ho $>$ Nd, Sm, La). Compounds **1** were dried in vacuo prior to each recrystallization to allow co-crystallized $AlMe_3$ to evaporate. (**CAUTION**: Volatiles containing trimethylaluminum react violently when exposed to air). $[Y(AlMe_4)_3]$ (**1a**), $[Ho(AlMe_4)_3]$ (**1g**), and $[Lu(AlMe_4)_3]$ (**1h**) were further purified by sublimation under the conditions reported in an earlier publication.[6] ^1H, ^{13}C, and ^{27}Al NMR spectroscopy as well as elemental analysis and IR spectroscopy confirmed the absence of $AlMe_3$ in complexes **1**. Due to efficient paramagnetic relaxation caused by the Ho^{3+} metal center, NMR spectroscopy was not informative for compound **1g**.

The cerium and praseodymium derivatives (**1c** and **1d**, respectively) were obtained following a slightly modified procedure (Scheme 2). Thus, commercially available anhydrous

$$LnCl_3 + 3\ LiNMe_2 \xrightarrow[RT,\ 18h]{toluene\ THF} [Ln(NMe_2)_3(LiCl)_3]$$

$$[Ln(NMe_2)_3(LiCl)_3] + 6\ AlMe_3 \xrightarrow[RT,\ 18h]{hexane} [Ln(AlMe_4)_3] + 1.5\ [\{Me_2AlNMe_2\}_2] + 3\ LiCl$$

Scheme 2. Synthesis of homoleptic rare-earth metal(III) tetramethylaluminates (Ln = Ce (**1c**), Pr (**1d**)).

metal trichlorides were used without previous activation by Soxhlet extraction.[25] After slow addition of THF to their toluene suspensions, three equivalents of solid $LiNMe_2$ were added to generate the dimethylamido ate complexes $[Ln(NMe_2)_3(LiCl)_3]$. A subsequent $AlMe_3$-mediated $[NMe_2]\rightarrow[AlMe_4]$ exchange in hexane gave compounds **1c** and **1d** in good yields. These tetramethylaluminate complexes were obtained as pale yellow (**1c**, 67%) or pale green (**1d**, 74%)

needles by recrystallization from saturated hexane solutions at −30 °C. Their compositions were confirmed by ^{1}H, ^{13}C, and ^{27}Al NMR spectroscopy (**1d**), elemental analysis, and IR spectroscopy. Due to efficient paramagnetic relaxation caused by the Ce^{3+} metal center, NMR spectroscopy was not informative for **1c**.

The high volatility of the alkylated amide by-product $[\{Me_2AlNMe_2\}_2]$ is one of the main advantages of this synthetic strategy. Although tetramethylaluminates are accessible by alkylation of a number of other Ln^{3+} precursor compounds, such as the readily available silylamide complexes $[Ln\{N(SiHMe_2)_2\}_3(thf)_2]$[26] or the tetrameric rare-earth metal neopentanolates $[\{Ln(OCH_2CMe_3)_3\}_4]$,[27] separation of the desired products from the alkylated by-products $[\{Me_2AlN(SiHMe_2)_2\}_2]$ and $[\{Me_2Al(OCH_2CMe_3)\}_2]$, respectively, which are non-volatile at ambient temperature, can prove difficult. For example, several recrystallizations from hexane solution at −30 °C are necessary to give pure $[Y\{(\mu\text{-}Me)_2AlMe_2\}_3]$ when synthesized according to Scheme 3. Furthermore, due to the higher bond energies of [Ln–O] versus [Ln–N] moieties, much larger excesses of $AlMe_3$ than the theoretical amount of six equivalents (Scheme 3) have to be added to give complexes **1** in acceptable yields.

$$[Ln\{N(SiHMe_2)_2\}_3(thf)_2] + 8\ AlMe_3 \xrightarrow[RT,\ 18h]{hexane} [Ln(AlMe_4)_3] + 1.5\ [\{Me_2AlN(SiHMe_2)_2\}_2] + 2\ Me_3Al(thf)$$

$$0.25\ [\{Ln(OCH_2CMe_3)_3\}_4] + 6\ AlMe_3 \xrightarrow[RT,\ 18h]{hexane} [Ln(AlMe_4)_3] + 1.5\ [\{Me_2Al(OCH_2CMe_3)\}_2]$$

Scheme 3. Alternative syntheses of homoleptic rare-earth metal tetramethylaluminates.

We also examined the feasibility of salt-metathesis reactions as one-step synthetic protocols for the preparation of complexes **1**. Thus, anhydrous (non-activated) YCl_3 and three equivalents of lithium tetramethylaluminate ($LiAlMe_4$) were suspended in a small amount of toluene and heated to 110 °C. However, after three days only 7% of $[Y\{(\mu\text{-}Me)_2AlMe_2\}_3]$ (**1a**) had formed as the only hexane-soluble rare-earth metal-containing product (Scheme 4). Attempts to synthesize the derivatives of the larger metals lanthanum and praseodymium failed. The reaction of anhydrous $LaCl_3$ with three equivalents of the toluene-soluble sodium tetraethylaluminate ($NaAlEt_4$), on the other hand, gave a small amount of a mixture of alkylated products (Scheme 4). Crystallization of the resulting products did not prove possible due to their high solubility.

$$YCl_3 + 3\ LiAlMe_4 \xrightarrow[110°C,\ 3\ days]{toluene} [Y(AlMe_4)_3] + 3\ LiCl$$

$$LaCl_3 + 3\ NaAlEt_4 \xrightarrow[110°C,\ 3\ days]{toluene} \text{mixture of alkylated products}$$

Scheme 4. Attempted syntheses of homoleptic rare-earth metal tetraalkylaluminate complexes by direct salt metathesis routes.

X-ray crystallographic studies of $Ln(AlMe_4)_3$: Single crystals of the homoleptic lutetium (**1h**), samarium (**1f**), praseodymium (**1d**), and lanthanum (**1b**) tetramethylaluminates suitable for X-ray crystallographic structure determinations were grown from saturated hexane solutions at −30 °C. This series covers the entire Ln^{3+} size range and thus allows an insight into any size-dependent aluminate coordination in the solid state. Isostructural $[Lu\{(\mu\text{-}Me)_2AlMe_2\}_3]$ (**1h**) and $[Sm\{(\mu\text{-}Me)_2AlMe_2\}_3]$ (**1f**), which represent the small to middle-sized Ln^{3+} ions, crystallize in the centrosymmetric space group *C*2/*c* (Figure 1, Table 1).

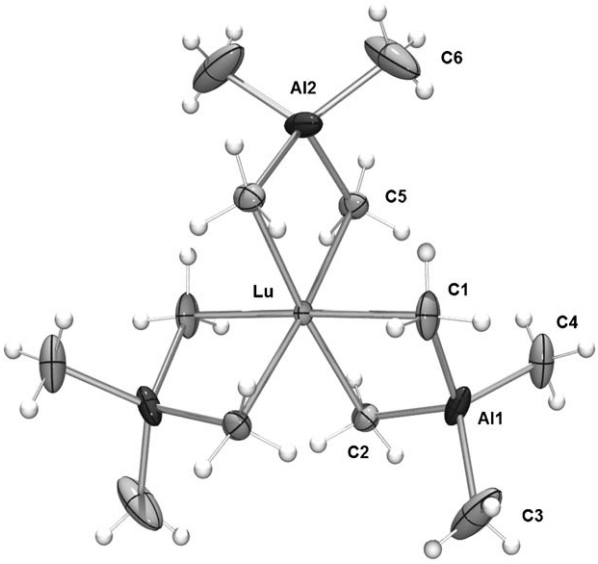

Figure 1. Molecular structure of **1h** (atomic displacement parameters set at the 50% level).

$[Pr\{(\mu\text{-}Me)_2AlMe_2\}_3]$ (**1d**), which features a slightly larger Pr^{3+} metal center (compared to Sm^{3+}), is isostructural with the previously reported neodymium derivative **1e** (monoclinic space group $P2_1/c$)[14] and crystallizes with two independent molecules in the unit cell (Figure 2, Table 2).

The solid-state structures of $[Ln(AlMe_4)_3]$ complexes (Ln = Lu, Sm, Pr, Nd) show a sixfold coordination of carbon atoms around the Ln^{3+} metal centers which results in a pseudo-octahedral geometry. Each $[AlMe_4]$ unit is coordinated to the central Ln metal through two methyl groups that bridge in an η^2 fashion and form planar or almost planar $[Ln(\mu\text{-}CH_3)_2Al]$ metallacycles (max. departure from least-squares planes: **1d**: −0.054(1) (Al4);**1f**: −0.0126(5) (Al1); **1h**: 0.001(1) Å (Al1)). Notably, the deviation from planarity, that is, the bending of the tetramethylaluminate ligand, increases with increasing metal size ($Pr^{3+} \approx Nd^{3+} > Sm^{3+} > Lu^{3+}$). All hydrogen atoms at the bridging methyl

Table 1. Selected bond lengths [Å] and angles [°] in compounds **1f** and **1h**.[a]

	$[Sm(AlMe_4)_3]$ (**1f**)	$[Lu(AlMe_4)_3]$ (**1h**)
Ln–C1	2.566(1)	2.466(2)
Ln–C2	2.573(1)	2.471(2)
Ln–C5	2.555(1)	2.455(2)
Al1–C1	2.086(1)	2.084(2)
Al1–C2	2.084(1)	2.078(2)
Al1–C3	1.968(2)	1.961(4)
Al1–C4	1.964(2)	1.964(2)
Al2–C5	2.091(2)	2.089(2)
Al2–C6	1.963(2)	1.961(5)
Ln–Al1	3.1323(3)	3.0176(5)
Ln–Al2	3.1207(5)	3.0062(8)
C1-Ln-C2	82.87(3)	86.30(7)
C1-Ln-C5	92.33(4)	89.01(7)
C1-Ln-C5′	90.25(4)	92.30(7)
C5-Ln-C5′	83.55(5)	87.05(7)
C1-Al1-C2	109.31(4)	108.44(9)
C5-Al2-C5′	108.93(6)	108.08(5)
C3-Al1-C4	118.69(6)	118.7(1)
C6-Al2-C6′	119.9(1)	119.7(2)

[a] Symmetry codes for equivalent atoms (′): $-x+1$, y, $1/2-z$ for **1f** and $-x$, y, $1/2-z$ for **1h**.

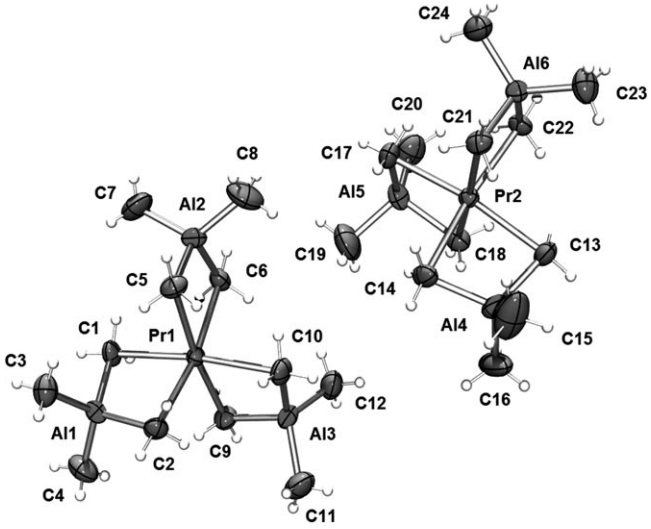

Figure 2. Molecular structure of **1d** (atomic displacement parameters set at the 50% level).

groups were located and refined to give five-coordinate carbon atoms with a heavily distorted trigonal-bipyramidal coordination geometry. Due to the steric unsaturation of the rare-earth metal center, two of the three H atoms in each bridging methyl group are directed toward the Ln atom. These hydrogen atoms and the aluminum occupy the equatorial positions of the trigonal bipyramid whereas the third hydrogen and the Ln metal are in the apical positions (e.g., Lu-C1-H13 169(2)°; Sm1-C1-H1B 168(1)°; Pr1-C1-H1C 172(2)°). The Ln–C(μ-Me) and Ln–Al bond lengths increase with increasing Ln^{3+} size but are shorter than the bonds in their half-metallocene $[(C_5Me_5)Lu\{(\mu\text{-}Me)_2AlMe_2\}_2]$ (av. Lu–C(μ) 2.505(3) and Lu–Al 3.0612(9) Å)[28] and metallocene $[(C_5Me_5)_2Sm\{(\mu\text{-}Me)AlMe_2(\mu\text{-}Me)\}_2Sm(C_5Me_5)_2]$ (av. Sm–C(μ) 2.75(1) and av. Sm–Al 4.792(5) Å)[29] derivatives. In accordance with the larger size of the Pr^{3+} ion compared to the neodymium derivative,[14] all of the Pr–C(μ-Me) bonds are slightly elongated (av. 2.604 Å (**1d**) vs. 2.589 Å (**1e**)).

$[La(AlMe_4)_3]$ (**1b**), which contains the largest Ln^{3+} ion, crystallizes in the monoclinic space group $P2_1/n$ with only one molecule in the unit cell. It exhibits an extraordinary solid-state structure (Figure 3) that features three different $[AlMe_4]$ coordination modes in a single molecule, namely $[La\{(\mu\text{-}Me)_2AlMe_2\}_2\{(\mu\text{-}Me)_3AlMe\}]$. One $AlMe_4^-$ ligand coordinates in the routinely observed η^2 fashion to form an almost planar heterobimetallic $[La(\mu\text{-}CH_3)_2Al]$ unit with a La1-C1-Al1-C2 torsion angle of 2.1(1)°. The second $AlMe_4^-$ ligand shows a bent η^2-coordination (La1-C9-Al3-C10 49.0(1)°) with an additional La–(μ-CH_3) contact (La1–C11 3.154(3) Å). The La–(μ-CH_3) bond lengths in this bent $AlMe_4^-$ ligand are elongated (Δ_{La-C} is approximately 0.119 Å) and the La1–Al3 distance is shortened (Δ_{La-Al} is approximately 0.232 Å). A similar structural motif has previously been found in the solid-state structures of $[(C_5Me_5)La(AlMe_4)_2]$[18] and $[(C_5Me_5)Lu(AlMe_4)_2]$.[28] Interestingly, the third $AlMe_4^-$ ligand coordinates through three bridging methyl groups to the lanthanum metal center. The La–(μ-CH_3) bonds (av. 2.882(6) Å) of this η^3-coordinated ligand are significantly longer than the bonds of the η^2-coordinated $[AlMe_4]$ moieties in **1b** and $[(C_5Me_5)La(AlMe_4)_2]$ (av. 2.749(7) Å).[18] In contrast, the La1–Al2 distance is shorter (2.995(1) Å) than the La1–Al1 (3.264(1) Å) and La1–Al3 (3.032(1) Å) distances. The differently coordinated tetramethylaluminate ligands lead to a coordination number of between seven and eight. As a comparison, chloroaluminate complexes of the type $[Ln(AlCl_4)_3]$ (Ln = Tb, Dy, Ho) exhibit a coordination number of eight by adopting a square-antiprismatic coordination geometry.[30] Very recently, the only other solid-state structure featuring such a true η^3-coordination of an $[AlMe_4]$ group to a rare-earth metal center was reported for the pentaneodymium cluster $[Cp^*_5Nd_5\{(\mu\text{-}Me)_3AlMe\}(\mu_4\text{-}Cl)(\mu_3\text{-}Cl)_2(\mu_2\text{-}Cl)_6]$.[31] The solid-state structure of $[La\{(\mu\text{-}Me)_2AlMe_2\}_2\{(\mu\text{-}Me)_3AlMe\}]$ proves the high coordinational flexibility of the tetramethylaluminate ligand and its ability to adapt perfectly to the given stereoelectronic requirements of the rare-earth metal center.

NMR spectroscopic investigations of $[Ln(AlMe_4)_3]$

Variable-temperature NMR studies and dynamic behavior: Despite their different solid-state structures, the ^1H NMR spectra of $[Ln\{(\mu\text{-}Me)_2AlMe_2\}_3]$ (Ln = Lu, Y, Sm, Nd) and $[La\{(\mu\text{-}Me)_2AlMe_2\}_2\{(\mu\text{-}Me)_3AlMe\}]$ show only one signal for the $[AlMe_4]$ moieties at ambient temperature. This is indicative of a very fast exchange of bridging and terminal methyl groups. However, two different types of methyl groups with an integral ratio of 1:1 could be resolved at lower temperature for the smaller Ln^{3+} complexes (Figure 4). Variable-temperature (VT) ^1H NMR experi-

Table 2. Selected bond lengths [Å] and angles [°] in compounds **1e**[14] and **1d**.

	$[Nd(AlMe_4)_3]$ (**1e**)	$[Pr(AlMe_4)_3]$ (**1d**)		$[Nd(AlMe_4)_3]$ (**1e**)	$[Pr(AlMe_4)_3]$ (**1d**)
	molecule 1			molecule 2	
Ln1−C1	2.578(13)	2.603(3)	Ln2−C13	2.581(14)	2.604(3)
Ln1−C2	2.563(14)	2.593(3)	Ln2−C14	2.596(13)	2.606(3)
Ln1−C5	2.605(13)	2.618(3)	Ln2−C17	2.566(14)	2.616(3)
Ln1−C6	2.609(14)	2.615(3)	Ln2−C18	2.595(14)	2.595(3)
Ln1−C9	2.601(14)	2.606(3)	Ln2−C21	2.594(13)	2.594(3)
Ln1−C10	2.595(13)	2.601(3)	Ln2−C22	2.588(13)	2.619(3)
Al1−C1	2.067(14)	2.087(3)	Al4−C13	2.075(14)	2.085(3)
Al1−C2	2.078(14)	2.092(3)	Al4−C14	2.076(13)	2.082(3)
Al1−C3	1.956(16)	1.958(3)	Al4−C15	1.971(18)	1.952(3)
Al1−C4	1.967(14)	1.961(3)	Al4−C16	1.944(15)	1.961(3)
Ln1−Al1	3.149(4)	3.1733(8)	Ln2−Al4	3.144(4)	3.1665(7)
Ln1−Al2	3.153(5)	3.1700(8)	Ln2−Al5	3.170(4)	3.1866(7)
Ln1−Al3	3.155(5)	3.1735(8)	Ln2−Al6	3.159(4)	3.1784(7)
C1-Ln1-C2	81.8(4)	81.82(8)	C13-Ln2-C14	82.0(4)	81.63(8)
C1-Ln1-C5	92.2(4)	92.35(8)	C13-Ln2-C17	94.7(4)	93.82(9)
C1-Ln1-C6	173.2(4)	172.67(9)	C13-Ln2-C18	174.4(5)	173.50(9)
C1-Ln1-C9	92.6(4)	93.06(8)	C13-Ln2-C21	92.4(4)	92.21(9)
C1-Ln1-C10	93.9(4)	93.55(9)	C13-Ln2-C22	91.2(4)	91.19(9)
C5-Ln1-C6	82.0(4)	81.19(9)	C17-Ln2-C18	81.0(4)	81.39(9)
C9-Ln1-C10	82.5(4)	81.33(9)	C21-Ln2-C22	81.4(4)	81.22(8)
C1-Al1-C2	108.6(6)	109.05(10)	C13-Al4-C14	109.8(5)	109.63(10)
C1-Al1-C3	107.3(6)	106.66(12)	C13-Al4-C15	106.8(7)	106.22(15)
C1-Al1-C4	107.4(6)	107.68(13)	C13-Al4-C16	107.6(7)	107.42(13)
C3-Al1-C4	118.9(7)	119.07(14)	C15-Al4-C16	119.1(8)	119.15(16)

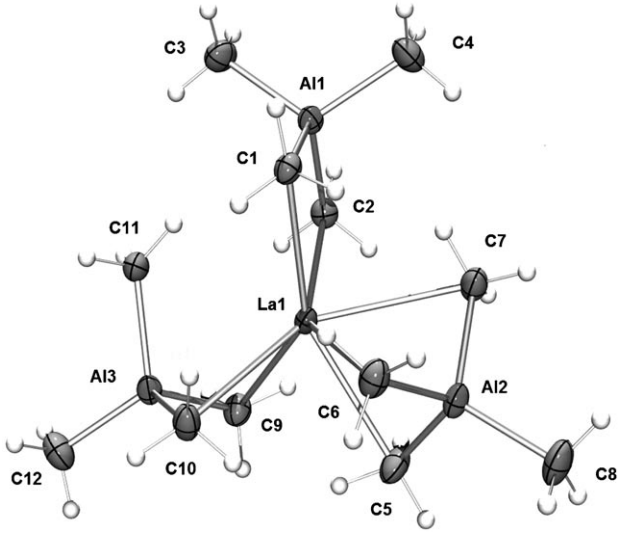

Figure 3. Molecular structure of **1b** (atomic displacement parameters set at the 50% level). Selected bond lengths [Å] and angles [°]: La1−C1 2.696(3), La1−C2 2.701(3), La1−C5 2.772(3), La1−C6 2.980(3), La1−C7 2.892(3), La1−C9 2.735(3), La1−C10 2.902(3), La1−C11 3.154(3), Al1−C1 2.080(3), Al1−C2 2.080(3), Al1−C3 1.972(3), Al1−C4 1.965(4), Al2−C5 2.056(4), Al2−C6 2.040(4), Al2−C7 2.036(4), Al2−C8 1.959(4), Al3−C9 2.072(4), Al3−C10 2.048(4), Al3−C11 2.001(3), Al3−C12 1.955(4), La1−Al1 3.264(1), La1−Al2 2.996(1), La1−Al3 3.032(1); C1-La1-C2 78.8(1), C1-La1-C5 114.4(1), C1-La1-C6 143.3(1), C1-La1-C7 80.3(1), C1-La1-C9 139.4(1), C1-La1-C10 80.9(1), C1-Al1-C2 110.9(2), C1-Al1-C3 106.6(2), C1-Al1-C4 109.2(2), C3-Al1-C4 114.3(2), C5-Al2-C6 107.1(1), C5-Al2-C7 103.6(2), C5-Al2-C8 112.5(2), C6-Al2-C8 112.6(2), C7-Al2-C8 114.8(2), C9-Al3-C10 108.1(2), C9-Al3-C11 103.8(2), C9-Al3-C12 112.7(2), C10-Al3-C11 106.1(2), C10-Al3-C12 110.55(2).

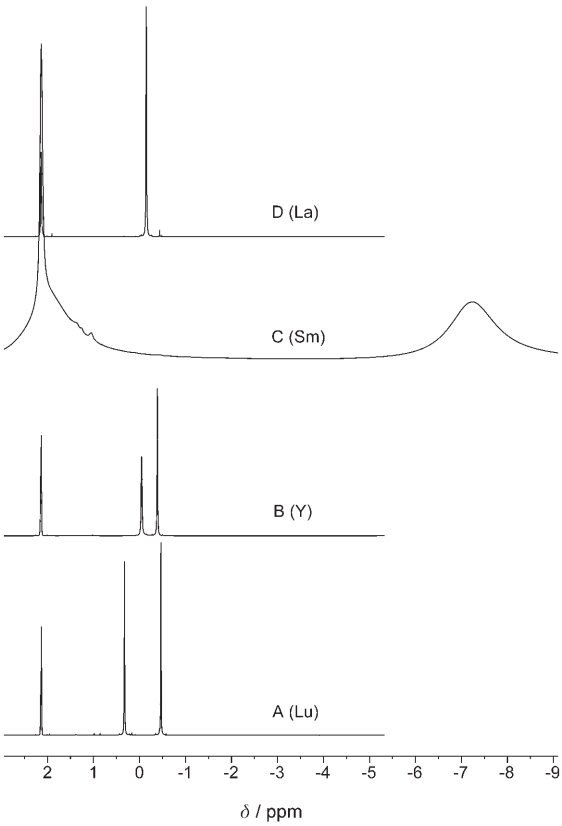

Figure 4. Low-temperature ^1H NMR spectra (500.13 MHz) of the methyl groups in A) $[Lu(AlMe_4)_3]$ (225 K), (B) $[Y(AlMe_4)_3]$ (193 K), (C) $[Sm(AlMe_4)_3]$ (191 K), and (D) $[La(AlMe_4)_3]$ (193 K) in $[D_8]$toluene (the residual protons of the toluene methyl group appear at $\delta = 2.1$ ppm).

ments in [D_8]toluene revealed decoalescence of the methyl resonances at a temperature, T_c, that decreases with increasing Ln^{3+} size (Lu = 278 > Y = 229 > Sm = 216 K). This is consistent with increased steric unsaturation and therefore more rapid alkyl exchange at the larger rare-earth metal centers.

Narrow signals with a 1:1 integral ratio for the two different methyl groups of [Ln{(μ-Me)$_2$AlMe$_2$}$_3$] (Ln = Lu, Y, Sm) were observed below 193 K (Figure 4). Broadening of the low-field methyl resonance of [Y{(μ-Me)$_2$AlMe$_2$}$_3$] due to a two-bond ^{1}H–^{89}Y scalar coupling ($^2J_{Y,H}$ = 2.5 Hz) was observed; this clearly shows that this signal is that of the bridging [(μ-Me)$_2$Al] moiety. Signal splitting of a considerably narrowed ^{1}H NMR resonance of the methyl groups occurred at temperatures well above coalescence (Figure 5a). This splitting, which reached optimal resolution at approximately 316 K, is clearly attributable to $^2J_{Y,H}$ coupling. Exceedingly fast methyl group exchange effectively appears to decouple the proton resonance at even higher temperatures, and at 348 K only a narrow singlet appears. It is noteworthy that the ^{13}C NMR spectrum at 193 K also shows two signals at δ = 13.7 and −8.5 ppm (Figure 5b). A ^{13}C–^{89}Y scalar coupling ($^1J_{Y,C}$ = 12.8 Hz) unambiguously confirms the low-field resonance as being that of the bridging [(μ-Me)$_2$Al] moiety. No decoalescence of the [AlMe$_4$] resonance was observed in the accessible temperature range (down to 183 K) for the largest lanthanide metal centers (Pr, Nd, and La). These findings are in good agreement with earlier investigations on the thermal behavior of [Ln(AlMe$_4$)$_3$] complexes.[14]

Structural evidence for a η^3-[AlMe$_4$] coordination in the solid state (see above) and the highly fluxional behavior of compounds **1** in solution suggest transient η^3-coordinated [AlMe$_4$] moieties for the larger Ln centers. A sterically unsaturated rare-earth metal center therefore allows for an associative methyl exchange, as depicted on the right-hand side of Figure 6, whereas in sterically hindered complexes

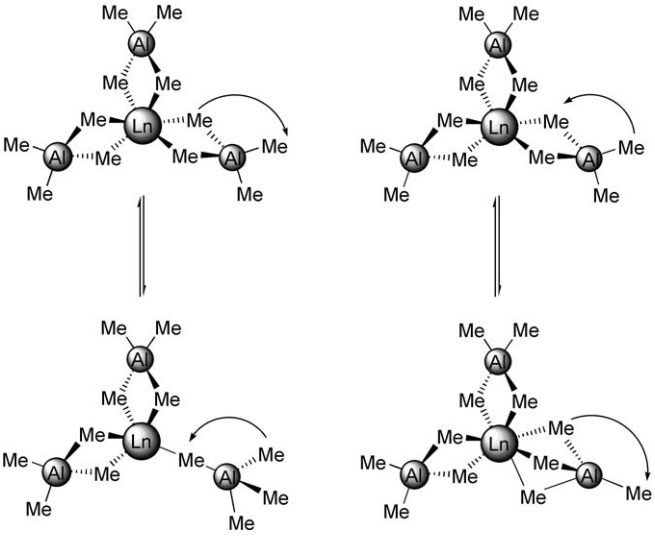

Figure 6. Dissociative (left) versus associative methyl exchange (right) in homoleptic [Ln(AlMe$_4$)$_3$] complexes.

such as [{(O$_2$CAr^{iPr})$_2$(μ-AlMe$_2$)}$_2$Y(AlMe$_4$)][16] (**2a**) and [Al$_2$Me$_6$][32] intramolecular methyl group exchange occurs via a dissociative mechanism with transient η^1-coordinated [AlMe$_4$] moieties, as shown on the left-hand side of Figure 6. The existence of such η^1-coordinated tetramethylaluminate ligands was recently confirmed by the solid-state structure of the diamidopyridine complex [(NNN)La{(μ-Me)AlMe$_3$}(thf)] (NNN = diaminopyridine).[21]

Dynamic NMR spectroscopy and line-shape analysis have proved to be a convenient tool for studying fast exchange processes in or between molecules and they have been successfully used to determine methyl exchange rates and activation parameters for several heteroleptic rare-earth metal tetramethylaluminate complexes.[16,28,33] A better understanding of the exchange mechanisms, kinetics, and thermodynamics of the homoleptic tetramethylaluminate complexes [Ln(AlMe$_4$)$_3$] could therefore be anticipated by applying dynamic NMR spectroscopy.

The ^{1}H NMR spectra of [Y(AlMe$_4$)$_3$] (**1a**), [Sm(AlMe$_4$)$_3$] (**1f**), and [Lu(AlMe$_4$)$_3$] (**1h**), as well as the ^{13}C NMR spectra

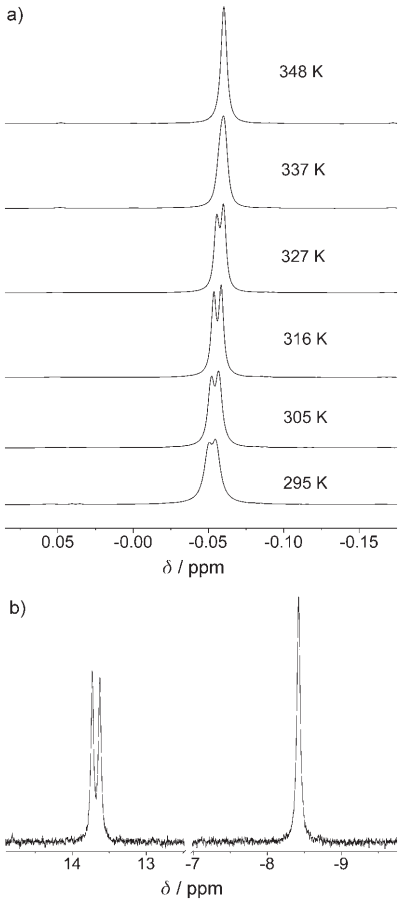

Figure 5. a) Variable-temperature ^{1}H NMR spectra (500.13 MHz) of [Y{(μ-Me)$_2$AlMe$_2$}$_3$] (**1a**) dissolved in [D_5]chlorobenzene in the temperature range 295–348 K; b) ^{13}C NMR spectrum (125.77 MHz) of **1a** dissolved in [D_8]toluene at 193 K.

of $[Y(AlMe_4)_3]$ (**1a**), were examined in different temperature ranges for solutions in $[D_8]$toluene. The rate constants of the methyl group exchange were obtained by simulating the NMR spectra with the program MEXICO.[34] This program simulates complex exchange spectra by taking into account homonuclear as well as heteronuclear scalar coupling and variations of the relative ^1H and ^{13}C chemical shifts of the two exchanging sites with temperature. A good fit to the experimental data parameters was obtained by using a procedure based on simplex iterations with a two-site mutual exchange model. Figures 7 and 8 show the experimental and

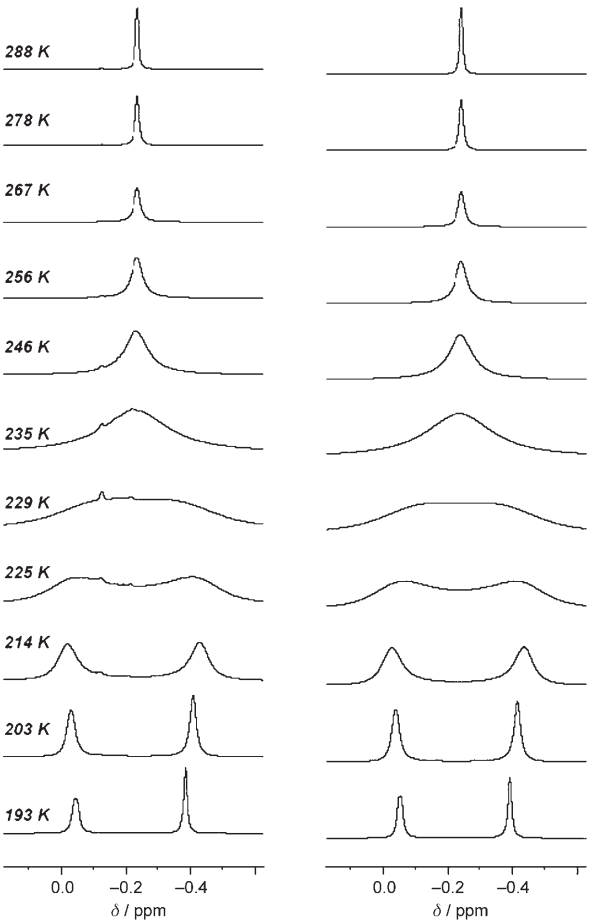

Figure 7. Experimental (left) and simulated (right) ^1H NMR spectra (500.13 MHz) of $[Y\{(\mu\text{-}Me)_2AlMe_2\}_3]$ (**1a**) in $[D_8]$toluene at different temperatures.

simulated line-shapes for the ^1H (500.13 MHz) and ^{13}C NMR (125.77 MHz) spectra of $[Y\{(\mu\text{-}Me)_2AlMe_2\}_3]$ (**1a**), respectively, at varying temperatures. The rate constants and values of the relevant thermodynamic parameters obtained in this work are summarized in Tables 3 and 4.

Even though the signal-to-noise ratios of some of the ^{13}C NMR spectra are very low, most notably close to coalescence, the calculated exchange rates show reasonable correspondence with those obtained by fitting the exchange model to the ^1H NMR spectra.

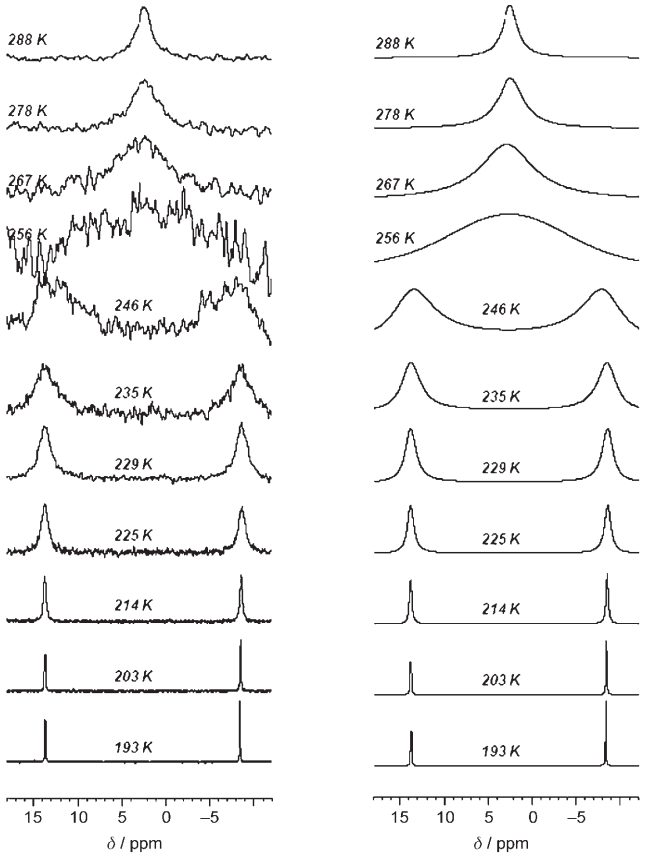

Figure 8. Experimental (left) and simulated (right) ^{13}C NMR spectra (125.77 MHz) of $[Y\{(\mu\text{-}Me)_2AlMe_2\}_3]$ (**1a**) in $[D_8]$toluene at different temperatures.

Surprisingly, the aluminate methyl group exchange proceeds with activation parameters (calculated using the Eyring equation; see also Figure 9) that indicate an associative methyl group exchange (right-hand side of Figure 6) for all $[Ln(AlMe_4)_3]$ complexes investigated. The negative activation entropies propose a higher ordered transition state, which implies an η^3-coordinated $[AlMe_4^-]$ ligand, for the complete series of Ln^{3+} ions. The activation entropy increases with decreasing size of the metal center, but appears to be lower for the smallest metal center lutetium than for yttrium. This could be due to strong secondary interactions, for example $Ln\cdots CH_3$ agostic interactions, originating from the most Lewis acidic Lu^{3+} center. For comparison, a dissociative methyl group exchange (positive $\Delta S^{\neq}$) has been reported for the $[Al_2Me_6]$ dimer[32] and the sterically crowded heteroleptic yttrium carboxylate complex **2a** (Table 4).[16] Moreover, the low $\Delta H^{\neq}$ values suggest relatively weak aluminate bonding.

In agreement with previous findings,[16] the free enthalpy decreases with increasing Ln^{3+} size, which is indicative of a weakening of the Ln–C bond for the larger metal centers. The comparatively higher free activation energy $\Delta G^{\neq}$ for the smallest metal center Lu compared to that for Sm at a given temperature corresponds to a slowing of the methyl group exchange. For example, a $\Delta(\Delta G^{\neq})$ value of

Table 3. Exchange rates k and free energies of activation ($\Delta G^{\neq}$) for [Lu($AlMe_4$)$_3$] (**1h**), [Sm($AlMe_4$)$_3$] (**1f**), and [Y($AlMe_4$)$_3$] (**1a**) obtained by line-shape analysis. The estimated uncertainty for the free energies of activation is 0.3 kJ mol^{-1}.

[Lu($AlMe_4$)$_3$] (**1h**)			[Sm($AlMe_4$)$_3$] (**1f**)			[Y($AlMe_4$)$_3$] (**1a**; ^{1}H NMR)			[Y($AlMe_4$)$_3$] (**1a**; ^{13}C NMR)	
T [K]	k [s^{-1}]	$\Delta G^{\neq}$ [kJ mol^{-1}]	T [K]	k [s^{-1}]	$\Delta G^{\neq}$ [kJ mol^{-1}]	T [K]	k [s^{-1}]	$\Delta G^{\neq}$ [kJ mol^{-1}]	k [s^{-1}]	$\Delta G^{\neq}$ [kJ mol^{-1}]
225	8.9	50.4	176	2.2×10^2	34.4	193	1.6×10^1	42.1	1.4×10^1	42.3
235	2.3×10^1	51.0	178	2.2×10^2	34.9	203	3.3×10^1	43.3	3.4×10^1	43.2
246	6.7×10^1	51.2	180	2.6×10^2	35.0	214	1.0×10^2	43.6	1.1×10^2	43.5
262	3.0×10^2	51.4	185	4.7×10^2	35.2	225	3.3×10^2	43.6	3.3×10^2	43.7
267	4.9×10^2	51.4	191	8.4×10^2	35.3	228	4.8×10^2	43.6	4.8×10^2	43.6
272	7.6×10^2	51.5	196	6.7×10^2	36.7	228	4.9×10^2	43.7	4.7×10^2	43.7
274	8.9×10^2	51.5	201	1.3×10^3	36.6	229	5.2×10^2	43.6	6×10^2	43.5
275	9.7×10^2	51.5	207	5.0×10^3	35.3	229	5.5×10^2	43.7	6×10^2	43.7
276	1.2×10^3	51.3	212	4.8×10^3	36.4	230	5.7×10^2	43.7	6×10^2	43.7
278	1.0×10^3	51.8	217	5.0×10^3	37.3	235	9.3×10^2	43.8	1.0×10^3	43.7
279	1.1×10^3	51.8	222	7.3×10^3	37.5	246	2.2×10^3	44.1	2.1×10^3	44.2
288	2.1×10^3	52.2	228	1.1×10^4	37.7	256	5.2×10^3	44.2	8×10^3	43.3
299	4.0×10^3	52.6	233	1.7×10^4	37.7	256	4.9×10^3	44.4	7×10^3	43.8
309	7.3×10^3	53.0	244	1.8×10^4	39.4	267	1.1×10^4	44.5	1.5×10^3	43.9
320	1.3×10^4	53.3	254	3.0×10^4	40.1	278	2.2×10^4	44.8	2.9×10^4	44.1
331	2.4×10^4	53.5	265	4.8×10^4	40.9	288	3.7×10^4	45.3	5×10^4	44.5
341	4.2×10^4	53.7	275	5.9×10^4	42.1					
352	5.7×10^4	54.6	286	9.3×10^4	42.8					
362	1.1×10^5	54.5	297	1.2×10^5	43.8					

Table 4. Thermodynamic data for the exchange of bridging and terminal methyl groups in [Ln($AlMe_4$)$_3$]- and [$AlMe_4$]-containing compounds. The activation parameters shown are only based on the variable ^{1}H NMR spectra.

Compound	T_c [K]	$\Delta G^{\neq}$ (T_c) [kJ mol^{-1}]	$\Delta H^{\neq}$ [kJ mol^{-1}]	$\Delta S^{\neq}$ [J K^{-1} mol^{-1}]
[Lu{(μ-Me)$_2$AlMe$_2$}$_3$] (**1h**)	279	51.8(3)	44(1)	−30(3)
[Y{(μ-Me)$_2$AlMe$_2$}$_3$] (**1a**)	229	43.6(3)	38(1)	−26(4)
[Sm{(μ-Me)$_2$AlMe$_2$}$_3$] (**1f**)	216	37.3(3)	20.2(6)	−78(3)
[(L^1)$_2$Y{(μ-Me)$_2$AlMe$_2$}] (**2a**)[a,d]	263	53(3)[c]	73(4)	66(3)
[(L^1)$_2$La{(μ-Me)$_2$AlMe$_2$}] (**2b**)[a,d]	213	45(2)[c]	28(2)	−58(3)
[(L^2)Y{(μ-Me)$_2$AlMe$_2$}][b,e]		63.0[c]	24.3	−130
[Me$_2$Al(μ-Me)$_2$AlMe$_2$][f]		44.8[c]	81.5	123.1

[a] L^1 = (O_2CAr^{iPr})$_2$(μ-$AlMe_2$). [b] L^2 = Me_2Si(2-MeBenzInd)$_2$. [c] At 298 K. [d] See ref. [16]. [e] See ref. [33]. [f] See ref. [32]

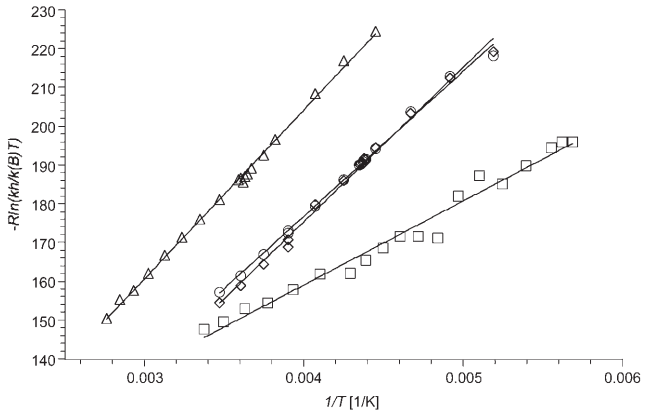

Figure 9. Linearized Eyring plots ($-R\ln(kh/k_BT) = -\Delta S^{\neq} + \Delta H^{\neq}/T$) for the exchange of bridging and terminal methyl groups in [Y($AlMe_4$)$_3$] ((◇), ^{1}H NMR data; (○), ^{13}C NMR data), [Lu($AlMe_4$)$_3$] (△), and [Sm($AlMe_4$)$_3$] (□).

9.4 kJ mol^{-1} at 275 K corresponds to a slowing by a factor 61 (Table 3).

1D ^{89}Y and 2D ^{1}H–^{89}Y NMR spectra of [Y($AlMe_4$)$_3$]: Metal-centered NMR spectroscopy is a particularly suitable probe of chemical reactivity as it is element specific and is applicable to any metal of the periodic table that has an isotope with a nuclear spin.[35] Additionally, metal nuclei have very large shielding (chemical shift) ranges and hence are very sensitive to small changes in geometry and coordination numbers, thereby revealing subtle changes in the solution composition of complexes. The properties of the monoisotopic ^{89}Y nucleus (100% abundance, $I = -1/2$, and a wide chemical shift range of approx. 1300 ppm) make it attractive for NMR studies. However, its routine use in the characterization of yttrium complexes is impaired by its low receptivity (0.681 relative to ^{13}C), low resonance frequency (24.5 MHz at a magnetic field strength of 11.7 T (^{1}H = 500 MHz)), and extremely long T_1 relaxation times (typically of the order of 60 s), which leads to lengthy experiments and saturation difficulties.

Contrary to chemical shift correlations in beryllium and aluminum complexes,[36,37] the correlation between ^{89}Y chemical shifts and the metal coordination number is unclear. Nevertheless, there are clear trends regarding the influence of various ligands on ^{89}Y chemical shifts. Thus, an increased electronegativity and π-donating ability of the ligated groups is correlated with increased ^{89}Y nuclear shielding and resonance shifts to higher field.[38] The chemical shifts of organoyttrium compounds extend over a very large range, with the most shielded cyclopentadienyl species in the range of about $\delta = -370$ (for [Y(C_5H_4Me)$_3$(thf)]) to 80 ppm; the

purely "σ-bound", and therefore most deshielded, species $[Y\{CH(SiMe_3)_2\}_3]$ has the largest reported chemical shift of +895 ppm (Table 5).

The ^{89}Y NMR spectrum of $[Y(AlMe_4)_3]$ (**1a**) as a 0.25 M solution in $[D_6]$benzene at 298 K shows a very narrow signal at $\delta = +394$ ppm (Figure 10). This value is best compared to the dicationic complexes $[Y(CH_2SiMe_3)(thf)_4][BPh_4]_2$ ($\delta =$ 409.2 ppm) and $[YMe(thf)_6][BPh_4]_2$ ($\delta = 433.2$ ppm) (Table 5), which are shifted substantially upfield from their neutral species. The relatively low-field shift of the ^{89}Y signal in the spectrum of $[Y(AlMe_4)_3]$ supports the conclusion that the aluminate bonding shows a significant degree of covalency.

This finding is in agreement with computational studies on the bonding nature in $[Y(AlMe_4)_3]$[42] and this covalent contribution to the Ln−C bond is further substantiated by the presence of a scalar ^1H–^{89}Y coupling. The resolvable $^2J_{Y,H}$ coupling was efficiently exploited in a two-dimensional ^1H–^{89}Y HMQC NMR experiment (0.25 M solution of **1a** in $[D_6]$benzene; Figure 10), which actually proved less time-consuming than the 1D ^{89}Y experiment (7 min vs. 2 h 20 min). Polarization transfer from ^1H to ^{89}Y greatly enhances the sensitivity and allows a much faster data accumulation rate which, in this case, is not restricted by the very long T_1 of ^{89}Y but rather the much shorter T_1 of ^1H.

^{27}Al NMR spectra of $[Ln(AlMe_4)_3]$ complexes: ^{27}Al NMR spectroscopy appears to be a very attractive technique for the study of Ln/Al heterobimetallic compounds as the ^{27}Al nucleus (100% abundance) has a relatively high magnetogyric ratio (similar to ^{13}C). However, the aluminum nucleus possesses a quadrupolar moment ($I = 5/2$) and hence often produces quite broad signals in the NMR spectra, with the linewidth depending heavily upon the coordination geometry of the aluminum metal center. The chemical shift range of ^{27}Al is approximately 450 ppm and chemical shifts can be categorized according to the ligand symmetry about the aluminum atom.[43] Aluminum species with tetrahedral symmetry, as in $[Ln(AlMe_4)_3]$ complexes, are found in an intermediate region of the chemical shift scale. Complexes with this symmetry are normally found at high frequency relative to $[Al(H_2O)_6]^{3+}$, with a chemical shift range extending from $\delta = -28$ ppm for $[AlI_4]^-$ to about $\delta = 220$ ppm for alkylaluminum complexes (Al_2R_6) and their adducts (Table 6).

Table 5. Alkylyttrium complexes and their corresponding ^{89}Y NMR chemical shifts.

Complex	δ_{exp} [ppm]	CN[a]	Solvent	Ref
$[\{Y(C_5H_4Me)_2(\mu\text{-}C{\equiv}CCMe_3)\}_2]$	−74	8	$[D_8]$THF	[39]
$[\{Y(C_5H_4Me)_2(\mu\text{-}Me)\}_2]$	−15	8	$[D_8]$toluene	[39]
$[Y(H_2O)_8]^{3+}$	0.00 (reference)	6	D_2O	
$[Y(C_5H_4Me)_2(Me)(thf)]$	40	8	$[D_8]$THF	[39]
$[Y(C_5Me_5)_2CH(SiMe_3)_2]$	78.9	4	$[D_6]$benzene	[38]
$[Y(CH_2SiMe_3)(thf)_4][BPh_4]_2$	409.2	5	$[D_8]$THF	[41]
$[YMe(thf)_6][BPh_4]_2$	433.2	7	$[D_5]$pyridine	[41]
$[Y\{1,3\text{-}(SiMe_3)_2C_3H_3\}_3]$	470.5	3	$[D_6]$benzene	[40]
$[Y(CH_2SiMe_3)_2(thf)_4][BPh_4]$	660.0	6	$[D_8]$THF	[41]
$[Y(CH_2SiMe_3)_2(thf)_4][BPh_3(CH_2SiMe_3)]$	660.2	6	$[D_8]$THF	[41]
$[Y(CH_2SiMe_3)_2(thf)_4][Al(CH_2SiMe_3)_4]$	666.4	6	$[D_8]$THF	[41]
$[Y(CH_2SiMe_3)_3(thf)_2]$	882.7	5	$[D_8]$THF	[41]
$[Y\{CH(SiMe_3)_2\}_3]$	895.0	3	$[D_8]$toluene	[38]

[a] CN = coordination number.

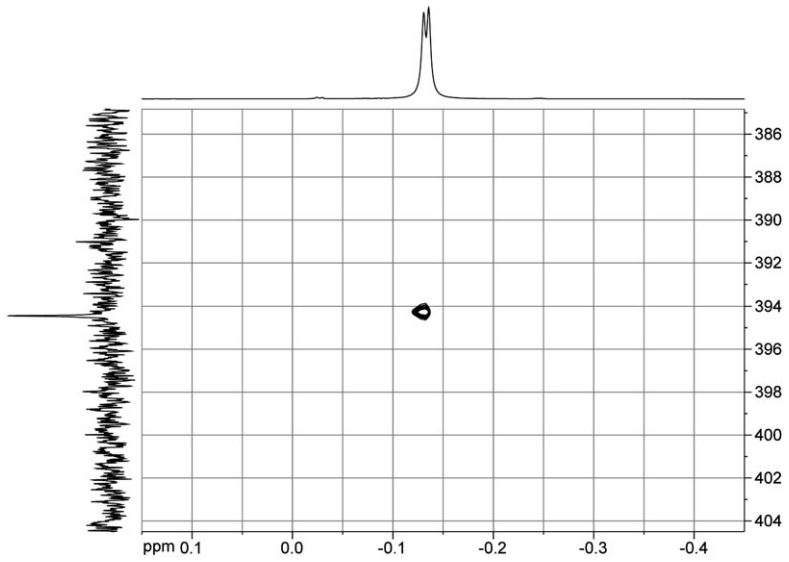

Figure 10. Two-dimensional ^1H–^{89}Y HMQC NMR spectrum of $[Y(AlMe_4)_3]$ (**1a**) dissolved in $[D_6]$benzene at 298 K. The 1D ^{89}Y NMR spectrum (24.51 MHz) is shown on the left edge of the contour plot and the 1D ^1H NMR spectrum (500.13 MHz) of the methyl region is shown at the top.

Good quality ^{27}Al NMR spectra of $[Ln(AlMe_4)_3]$ (Ln = Y, La, Pr, Nd, Sm, and Lu) complexes as 0.25 M solutions in $[D_6]$benzene could be acquired at 25 °C within a short time (Figure 11). All spectra show a single ^{27}Al NMR peak with linewidths between $\Delta\nu_{1/2} =$ 1836 Hz for $[Sm(AlMe_4)_3]$ and 3150 Hz for $[Y(AlMe_4)_3]$. Since all the Al atoms maintain their fourfold coordination, these relatively large linewidths could arise from associative methyl group exchange, which would lead to a pronounced distortion from tetrahedral symmetry.[47] The chemical shifts of the Lu ($\delta = 163$ ppm), Y ($\delta = 167$ ppm), Sm ($\delta = 163$ ppm), and La ($\delta =$ 165 ppm) derivatives are in the expected region for tetrahedral-

Table 6. Aluminum compounds and their corresponding ^{27}Al chemical shifts and linewidths.

Compound	δ_{exp} [ppm]	Solvent	Linewidth [Hz]	Ref
$Et_3Al{\cdot}SEt_2$	+221	C_6H_{12}	1890	[44]
$[Al_2iBu_6]$	+220	C_6H_{12}	6000	[45]
$Et_3Al{\cdot}thf$	+176	C_6H_{12}	1280	[44]
$[AlHiBu_2]_n$	+162		10000	[45]
$[Al_2Et_6]$	+171	C_6H_{12}	1700	[45]
$[Al_2Me_6]$	+156	neat	450	[45]
$[Al(H_2O)_6]^{3+}$	0	H_2O	3	[46]

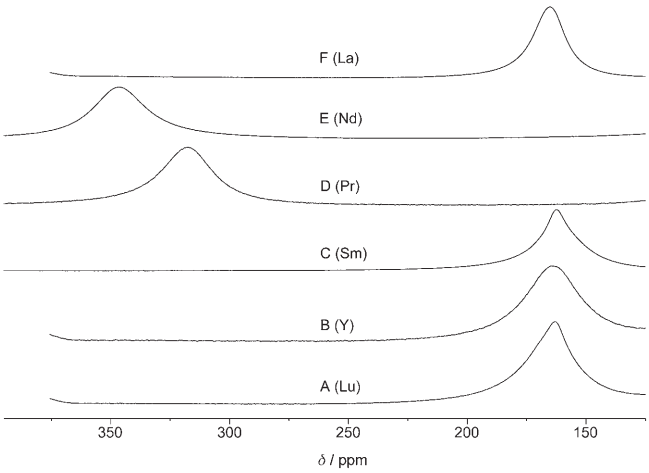

Figure 11. ^{27}Al NMR spectra (130.32 MHz) of $[Lu(AlMe_4)_3]$ (A), $[Y(AlMe_4)_3]$ (B), $[Sm(AlMe_4)_3]$ (C), $[Pr(AlMe_4)_3]$ (D), $[Nd(AlMe_4)_3]$ (E), and $[La(AlMe_4)_3]$ (F) dissolved in $[D_6]$benzene at 298 K.

ly coordinated alkylaluminum complexes and they differ only slightly from the chemical shifts reported for $[Al_2Me_6]$ and $[Al_2Et_6]$ (Table 6). Exceptionally low-field shifts of $\delta =$ 317 and 346 ppm, most likely caused by the paramagnetic metal centers, were obtained for $[Pr(AlMe_4)_3]$ (**1d**) and $[Nd(AlMe_4)_3]$ (**1e**), respectively. The paramagnetic shift effect on the ^{27}Al signal in $[Sm(AlMe_4)_3]$ is negligible. The paramagnetic Ln^{3+} metal centers influence the ^{27}Al NMR spectra differently, and these differences are probably due to the varying relaxation behavior of the unpaired electron spins belonging to the paramagnetic metal centers. Pr^{3+} and Nd^{3+} seem to cause a significant paramagnetic shift for the ^{27}Al resonances, although no broadening effect is observed. Neither of these influences are pronounced for the ^{27}Al signals of $[Sm(AlMe_4)_3]$, although possible paramagnetic shifts and broadening effects are observed in the ^1H (Figure 4) and ^{13}C NMR spectra (not shown) of $[Sm(AlMe_4)_3]$. None of the various paramagnetic effects were investigated further. As expected, due to fast (T_2) relaxation of the ^{27}Al nuclear spin and the concomitant line-broadening, spin-spin coupling was not observed in the NMR spectra.

Reactivity toward carboxylic acids and silanols: As shown previously, homoleptic $[Ln(AlMe_4)_3]$ complexes readily undergo protonolysis reactions with a variety of Brønsted acidic O-donors, including phenols, alcohols, silanols, and carboxylic acids, to generate heteroleptic Ln/Al heterobimetallic complexes.[16,17] These complexes not only show an interesting structural chemistry but can also act as model systems to study structure–reactivity relationships in commonly used Ziegler-type catalysts. The alkylated heterobimetallic lanthanide carboxylate complexes $[Ln\{(O_2CAr^{iPr})_2(\mu\text{-}AlMe_2)\}_2(AlMe_4)(C_6H_{14})]$ (Figure 12) and $[\{Ln(O_2CC_6H_2\text{-}tBu_3\text{-}2,4,6)\{(\mu\text{-}Me)_2AlMe_2\}_2\}_2]$, derived from the sterically bulky 2,4,6-triisopropyl- and 2,4,6-tri-*tert*-butylbenzoic acids, respectively, have been prepared from **1** in good to quantitative yields by methane elimination reactions.[16]

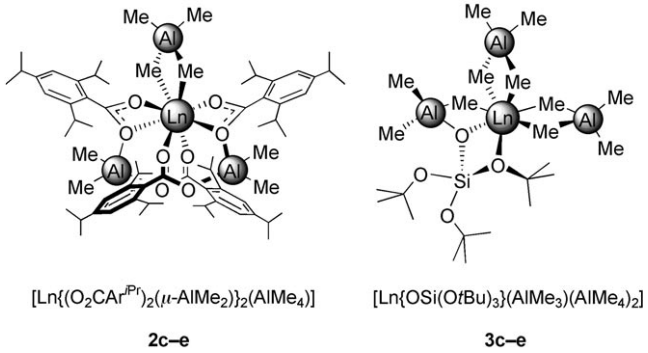

Figure 12. Heteroleptic carboxylate and siloxide complexes of Ce, Pr, and Nd synthesized from **1** by methane elimination and used as precatalysts in isoprene polymerization.

This strategy was also successfully employed here to synthesize the cerium and praseodymium complexes **2c** and **2d**, respectively (Scheme 5). Thus, homoleptic tetramethylalumi-

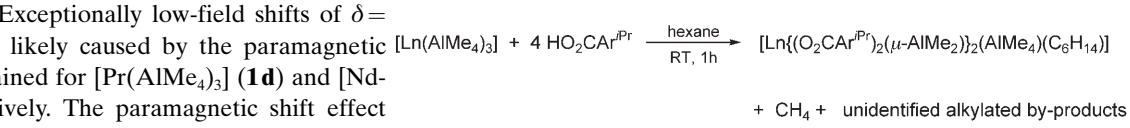

Scheme 5. Synthesis of alkylaluminum lanthanide carboxylates ($Ar^{iPr} = C_6H_2iPr_3$-2,4,6; Ln = Ce (**2c**), Pr (**2d**), Nd (**2e**)).

nate complexes **1c** and **1d** were treated with four equivalents of solid 2,4,6-triisopropylbenzoic acid. After the evolution of methane had ceased (< 5 min) the clear solutions were stirred for one hour, concentrated, and finally stored overnight at −30 °C to give pale-yellow (Ln = Ce (**2c**)) or pale-green (Ln = Pr (**2d**)) crystalline solids in good yields.

The elemental analyses of **2c** and **2d** were in good agreement with the formation of hexane inclusion compounds, and one equivalent of hexane remained confined within the crystal lattice even under high vacuum. The same observation has previously been made for the derivatives of lanthanum, neodymium, and gadolinium and proven by means of elemental analysis and NMR spectroscopy (for Ln = La).[16] On the other hand, hexane-insoluble homologues with no

residual solvent molecules have been obtained for the smaller metal centers yttrium and lutetium.[48]

The reaction of homoleptic tetramethylaluminate complexes **1c**, **1d**, and **1e** with one equivalent of tris(*tert*-butoxy)silanol ($HOSi(OtBu)_3$) afforded the heteroleptic siloxide complexes $[Ln\{OSi(OtBu)_3\}(AlMe_3)(AlMe_4)_2]$ (**3c**–**e**) (Figure 13 and Scheme 6).[17,49] The new cerium and praseodymium derivatives **3c** (Ln = Ce) and **3d** (Ln = Pr) were obtained in good yields. Recrystallization from saturated hexane solutions at −30 °C gave pale yellow (**3c**) and pale green (**3d**) crystals which gave correct elemental analyses.

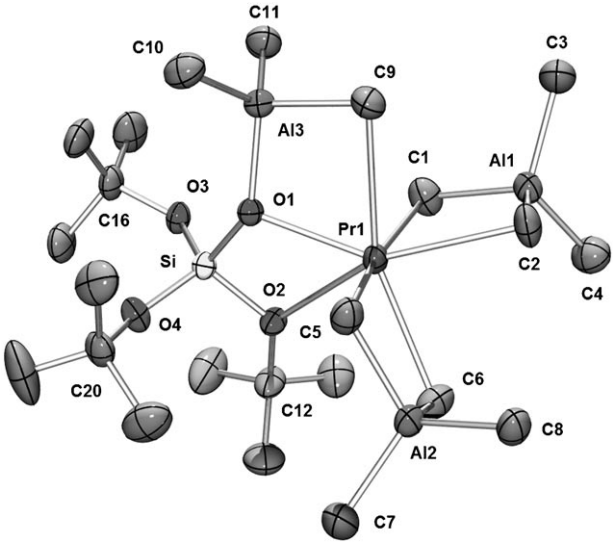

Figure 13. Molecular structure of **3d** (atomic displacement parameters set at the 50% level). Hydrogen atoms have been omitted for clarity. Selected bond lengths [Å] and angles [°]: Pr1−C1 2.619(3), Pr1−C2 2.795(3), Pr1−C5 2.676(3), Pr1−C6 2.621(3), Pr1−C9 2.754(3), Pr1−O1 2.357(2), Pr1−O2 2.714(2), Al1−C1 2.082(4), Al1−C2 2.070(4), Al1−C3 1.967(4), Al1−C4 1.965(4), Al3−C9 2.042(4), Al3−C10 1.952(3), Al3−C11 1.968(3), Al3−O1 1.854(2), Si−O1 1.629(2), Si−O2 1.660(2), Si−O3 1.600(2), Si−O4 1.595(2); C1-Pr1-C2 78.6(1), C1-Pr1-C5 167.8(1), C1-Pr1-C6 101.1(1), C1-Pr1-C9 88.1(1), C2-Pr1-C5 89.6(1), C2-Pr1-C6 79.1(1), C2-Pr1-C9 76.0(1), C5-Pr1-C6 79.2(1), C5-Pr1-C9 86.2(1), C6-Pr1-C9 151.1(1), O1-Pr1-O2 57.13(6), O1-Pr1-C1 99.5(1), O1-Pr1-C2 146.6(1), O1-Pr1-C5 88.7(1), O1-Pr1-C6 133.1(1), O1-Pr1-C9 70.6(1), O2-Pr1-C1 84.8(1), O2-Pr1-C2 152.9(1), O2-Pr1-C5 107.3(1), O2-Pr1-C6 83.4(1), O2-Pr1-C9 125.0(1).

$$[Ln(AlMe_4)_3] + HOSi(OtBu)_3 \xrightarrow[RT,\ 1h]{hexane} [Ln\{OSi(OtBu)_3\}(AlMe_3)(AlMe_4)_2] + CH_4$$

Scheme 6. Synthesis of alkylaluminum lanthanide siloxides (Ln = Ce (**3c**), Pr (**3d**), Nd (**3e**)).

The single crystals of **3d** proved to be suitable for an X-ray crystallographic structure determination. As reported previously for the lanthanum derivative,[17,49] the praseodymium metal center is seven-coordinated by five $AlCH_3$ carbon atoms and two oxygen atoms of an asymmetrically η^2-coordinated siloxide ligand (Figure 13). One of the tetramethylaluminate units is asymmetrically coordinated due to the pseudo-*trans* positions of the siloxide ligand within the distorted pentagonal bipyramid. A significantly elongated Pr1−C2 bond (2.795(3) Å) is present compared to the average Pr−C(μ-Me) distances in **1d** (2.606 Å) and **3d** (2.667 Å, $AlMe_4$ units except for Pr1−C2). This distance is even larger than the Pr1−C9 distance of the coordinated $AlMe_3$ molecule (2.754(3) Å). Nevertheless, both $[Pr(\mu\text{-}Me)_2AlMe_2]$ metallacycles remain planar, with sums of the inner bond angles of 359.9(2)° and 359.8(2)°, respectively.

Type-**3** siloxide derivatives have been discussed as possible model complexes for the reaction of **1** with a dehydrated silica surface, and grafting of the binary $[Nd(AlMe_4)_3]$/Et_2AlCl precatalyst system onto mesoporous silica MCM-48 has yielded a very efficient single-component catalyst for the *cis*-stereospecific polymerization of isoprene.[17,50]

Polymerization of isoprene: Complexes **1**, **2**, and **3** (Figure 12) were employed as precatalysts in the *cis*-stereospecific polymerization of isoprene. Diethylaluminum chloride (Et_2AlCl) was used as a co-catalyst and the formation of high-*cis*-1,4-polyisoprene (>98%) was proven by ^{13}C NMR spectroscopy. Emphasis was placed on the impact of the metal center and the n_{Ln}:n_{Cl} ratios on polymer yields, molecular weights, and molecular weight distributions. The polymerization results are summarized in Table 7 along with the data for the neodymium-based catalysts taken from previous studies, which were performed under similar conditions (see Experimental Section).[16,17] All of the precursor molecules display n_{Ln}:n_{Al} ratios of 1:3, although the heterobimetallic carboxylate complexes **2** contain oxygen-bonded "deactivated" dimethylaluminum bridges.

Impact of the metal center on the catalytic activity: The metal centers cerium, praseodymium, and neodymium were selected to investigate the intrinsic "neodymium effect" more systematically. In previous studies we have shown that neodymium alkylaluminate complexes greatly outperform their corresponding lanthanum and gadolinium congeners (Figure 14).[16] Unsurprisingly for complexes derived from large rare-earth metal centers, the cerium and praseodymium derivatives **1**–**3** are also highly active initiators in isoprene polymerization.[51,52] Almost all of the tetramethylaluminate complexes **1** gave quantitative yields of high-*cis*-1,4-polyisoprenes in the presence of between one and three equivalents of the alkylaluminum chloride co-catalyst (Table 7, runs 1–9). The slightly lower activities of the carboxylate- and siloxide-based initiators allow for a more detailed discussion of the metal effect. For example, the heterobimetallic lanthanide carboxylate complexes **2** produce polyisoprenes in yields of 79% (**2c**, Ln = Ce, run 10), 98% (**2d**, Ln = Pr, run 13), and 77% (**2e**, Ln = Nd, run 16) upon addition of one equivalent of Et_2AlCl. These findings "complete" a previous study where catalysts derived from larger (Ln = La, 12%) and smaller metal centers (Ln = Gd, 24%) gave lower yields of isolated polymer (Figure 14).[16]

Table 7. Results of the polymerization of isoprene using compounds **1**–**3** in combination with different amounts of Et_2AlCl as co-catalyst.

Run[a]	Precatalyst	Et_2AlCl[b] [equiv]	Yield [%]	M_n[c] ($\times 10^3$)	M_w[c] ($\times 10^3$)	PDI[c]
1	**1c** (Ce)	1	>99	160	386	2.41
2	**1c** (Ce)	2	>99	152	469	3.08
3	**1c** (Ce)	3	13	66	241	3.66
4	**1d** (Pr)	1	>99	386	732	1.90
5	**1d** (Pr)	2	>99	320	735	2.30
6	**1d** (Pr)	3	>99	345	704	2.02
7	**1e** (Nd)	1	>99	228	788	3.45
8	**1e** (Nd)	2	>99	117	326	2.78
9	**1e** (Nd)	3	>99	113	329	2.92
10	**2c** (Ce)	1	79	187	418	2.24
11	**2c** (Ce)	2	>99	149	532	3.59
12	**2c** (Ce)	3	97	256	494	1.93
13	**2d** (Pr)	1	98	573	863	1.51
14	**2d** (Pr)	2	>99	158	650	4.11
15	**2d** (Pr)	3	>99	476	778	1.64
16	**2e** (Nd)	1	77	165	575	3.48
17	**2e** (Nd)	2	> 99	271	621	2.29
18	**2e** (Nd)	3	98	194	410	2.11
19	**3c** (Ce)	1	18	414	744	1.80
20	**3c** (Ce)	2	>99	535	807	1.51
21	**3c** (Ce)	3	33	72	366	5.08
22	**3d** (Pr)	1	21	303	718	2.37
23	**3d** (Pr)	2	>99	446	762	1.71
24	**3d** (Pr)	3	88	354	707	2.00
25	**3e** (Nd)	1	92	355	744	2.10
26	**3e** (Nd)	2	>99	223	453	2.03
27	**3e** (Nd)	3	38	107	371	3.46

[a] General polymerization procedure: 0.02 mmol of precatalyst, 8 mL of hexane, 0.02–0.06 mmol of Et_2AlCl (1–3 equiv), 20 mmol of isoprene; 24 h, 40 °C. [b] Catalyst pre-formation: 30 min at ambient temperature. [c] Determined by size-exclusion chromatography (SEC) against polystyrene standards.

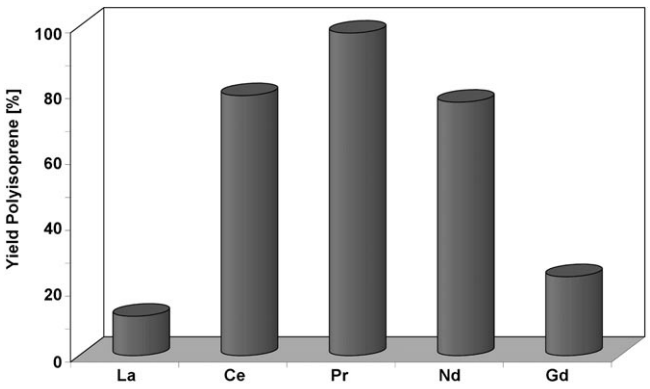

Figure 14. Yields of isolated polyisoprene obtained with carboxylate precatalysts **2** and one equivalent of Et_2AlCl co-catalyst. Data for the La, Nd, and Gd polymerizations are taken from previous studies performed under similar conditions.[17]

No neodymium effect was observed in the presence of three equivalents of the co-catalyst for either carboxylate (Table 7, runs 12, 15, and 18) or siloxide precatalysts (Table 7, runs 21, 24, and 27).

Impact of the metal center on the polymer properties: Higher molecular weights were obtained, on average, for praseodymium-based initiators with identical ligand environments and the same amount of co-catalyst. For example, homoleptic tetramethylaluminate complexes **1** gave molecular weights, M_w, of 241000 (Ln = Ce, run 3), 704000 (Ln = Pr, run 6), and 329000 g mol^{-1} (Ln = Nd, run 9) upon activation with three equivalents of Et_2AlCl. The polydispersities do not show any clear trend and range from 1.51 (runs 13 and 20) to 5.08 (run 21).

Impact of the ligand on the catalytic activity: Quantitative polymer formation was observed in almost all of the experiments based on **1** (Table 7, runs 1–9), thus showing the superior performance of the homoleptic complexes compared to all of the other precatalysts employed in this and earlier studies.[17] Only in the presence of **1c** (Ln = Ce) and three equivalents of the chloride co-catalyst, a drastically lower activity with an isolated yield of only 13% was observed (run 3). For comparison, the slightly larger metal center lanthanum gave catalytically inactive mixtures under similar conditions.[17] The carboxylate- and particularly the siloxide-derived initiators revealed significantly lower catalytic activities in the presence of one or three equivalents of the co-catalyst. Surprisingly, higher activities were observed for the mono(tetramethylaluminate) complexes **2** (Table 7, runs 10–18) than for the bis(tetramethylaluminate) complexes **3** (Table 7, runs 19–27).

Impact of the ligand on the polymer properties: Despite the stereoelectronic differences between alkylaluminate, carboxylate, and siloxide ligands, the molecular weights and molecular weight distributions are very similar, although slightly shorter polymer chains are generally produced by the most reactive tetramethylaluminate precatalysts **1** (Table 7, runs 1–9).

Impact of the catalyst-to-co-catalyst ratio on the catalytic activities: As reported previously for a variety of different initiator systems based on halide, carboxylate, alkoxide, and phosphate ligands, the highest polymer yields were obtained in the presence of two equivalents of the Et_2AlCl co-catalyst.[53–57] Quantitative yields of *cis*-1,4-polyisoprene were obtained for all of the precatalysts, regardless of the size of the lanthanide metal center or the type of ligand system. This study demonstrates once again that the presence of two equivalents of the chloride source seems to be crucial for optimal activation of the rare-earth metal centers. Lower reactivities were observed in the presence of three equivalents of the chloride source due to the formation of larger amounts of perhalogenated, and therefore catalytically inactive, $LnCl_3$.

Impact of the catalyst-to-co-catalyst ratio on the polymer properties: The molecular weights and molecular weight distributions of all the polymers obtained seem to follow no general trend—both values are actually more dependent on the size of the metal center and the type of ligand environment under similar conditions (see above).

Conclusion

Amide elimination has been confirmed as the optimal approach to homoleptic rare-earth metal tris(tetramethylaluminate) complexes. $[Ln(AlMe_4)_3]$ complexes with metals in the $La^{3+}\rightarrow Lu^{3+}$ size range can be straightforwardly obtained by the reaction of $[Ln(NMe_2)_3(LiCl)_3]$ with trimethylaluminum. X-ray structure analyses of the lutetium, samarium, praseodymium, and lanthanum tetramethylaluminates have revealed a Ln^{3+} cation size-dependent coordination of the $[AlMe_4]$ moieties. The exceptional solid-state structure of the lanthanum derivative can best be described by the formula $[La\{(\mu\text{-}Me)_2AlMe_2\}_2\{(\mu\text{-}Me)_3AlMe\}]$, which involves $AlMe_4^-$ ligands coordinating in three different coordination modes. The resulting higher coordination number of the lanthanum center ($6\rightarrow 7/8$) certainly reflects the larger La^{3+} size, but also corroborates the high coordinational flexibility of the tetramethylaluminate ligand. AlR_4^- ligands therefore seem to willingly adapt to the stereoelectronic requirements of the complex they find themselves in, gradually changing along the Ln series by undergoing $\eta^2\rightarrow\eta^3$ (steric unsaturation, this work) and $\eta^2\rightarrow\eta^1$ coordination shifts (steric oversaturation). The former $Ln[(\mu\text{-}Me)_2AlMe_2]\rightarrow Ln[(\mu\text{-}Me)_3AlMe]$ ($\eta^2\rightarrow\eta^3$) coordination mode shift characterizing the associative methyl exchange between bridging and terminal methyl groups has also been observed by dynamic ^1H and ^{13}C NMR spectroscopy by utilizing line-shape analysis in which higher ordered transient states (η^3) are indicated by negative values of $\Delta S^{\neq}$. The presence of a $^2J_{Y,H}$ (2.5 Hz) and a $^1J_{Y,C}$ (12.8 Hz) scalar coupling provides evidence for a significant degree of covalency of the Ln-aluminate bonding. In addition, the $^2J_{Y,H}$ coupling allows for a fast and thereby sensitive alternative to obtaining ^{89}Y chemical shifts. The ^{27}Al NMR spectra of $[Ln(AlMe_4)_3]$ complexes have revealed a drastic low-field shift for the paramagnetic neodymium and praseodymium derivatives. Finally, isoprene polymerization utilizing three types of structurally well-defined heterobimetallic rare-earth metal complexes of the large metal centers Ce, Pr, and Nd with alkylaluminate, carboxylate, and siloxide ligands has revealed: a) high activities in the presence of diethylaluminum chloride as a co-catalyst (optimal ratio $n_{Ln}:n_{cocatalyst}=1:2$), b) a *cis* stereospecificity for all the initiators of more than 98%, c) the superior performance of homoleptic $[Ln(AlMe_4)_3]$ complexes compared to carboxylate and siloxide derivatives, and d) that the "intrinsic neodymium effect", that is, the fact that the highest activities in diene polymerizations so far have been observed for neodymium-based catalyst systems, has to be put into perspective.

Experimental Section

General remarks: All operations were performed with rigorous exclusion of air and water using standard Schlenk, high-vacuum, and glove box techniques (MBraun MBLab; <1 ppm O_2, <1 ppm H_2O). Hexane, THF, and toluene were purified with Grubbs columns (MBraun SPS, solvent purification system) and stored in a glove box. $[D_6]$Benzene was obtained from Aldrich, degassed, dried with Na for 24 h, and filtered. $AlMe_3$ and Et_2AlCl were purchased from Aldrich and used as received. Isoprene was obtained from Aldrich, dried several times over activated molecular sieves (3 Å) and distilled prior to use. Complexes **1b**,[17] **1h**,[6] **2e**,[48] and **3e**[17] were synthesized according to previously published procedures. $LiAlMe_4$ and $NaAlEt_4$ were prepared according to literature procedures.[58,59] IR spectra were recorded with a NICOLET Impact 410 FTIR spectrometer and a Perkin–Elmer 1650 FTIR spectrometer as Nujol mulls sandwiched between CsI plates. Elemental analyses were performed with an Elementar Vario EL III.

General procedure for the synthesis of lanthanide(III) tris(tetramethylaluminate)s 1a, 1e, 1f, and 1g: A THF solution of three equivalents of $LiNMe_2$ (10 mL) was added slowly to a suspension of $[LnCl_3(thf)_x]$ in THF (15 mL) and the mixture was stirred at ambient temperature for 18 h. The solvent was then removed in vacuo. The remaining solid was suspended in hexane, a solution containing eight equivalents of $AlMe_3$ diluted with hexane was added, and the resulting mixture stirred at ambient temperature. After 18 h the solvent was removed under reduced pressure, the residue extracted several times with hexane, and the product separated by crystallization at −30 °C. The $[Ln(AlMe_4)_3]$ complex was recrystallized several times from hexane at −30 °C to obtain $AlMe_3$-free crystals, which were dried in vacuo prior to each recrystallization cycle.

Yttrium(III) tris(tetramethylaluminate) (1a): Following the procedure described above, $[YCl_3(thf)_{3.5}]$ (6.10 g, 13.62 mmol), $LiNMe_2$ (2.09 g, 40.87 mmol), and $AlMe_3$ (7.86 g, 108.99 mmol) yielded **1a** as colorless crystals (4.30 g, 12.26 mmol, 90%). ^1H NMR (600 MHz, $[D_6]$benzene, 25 °C): $\delta=-0.25$ (s, $Al(CH_3)_4$) ppm. ^1H NMR (500 MHz, $[D_8]$toluene, 25 °C): $\delta=-2.4$ (s, $Al(CH_3)_4$) ppm. ^{13}C NMR (151 MHz, $[D_6]$benzene, 25 °C): $\delta=2.8$ (brs, $Al(CH_3)_4$) ppm. ^{27}Al NMR (130 MHz, $[D_6]$benzene, 25 °C): $\delta=167$ (brs, $\Delta\nu_{1/2}=3150$ Hz, $Al(CH_3)_4$) ppm. IR (nujol): $\tilde{\nu}=1463$ (vs, nujol), 1385 (vs, nujol), 1303 (w), 1225 (s), 1204 (vs), 971 (w), 899 (w), 852 (w), 733 (vs), 707 (vs), 578 (vs), 557 cm^{-1} (vs). Elemental analysis (%) calcd for $C_{12}H_{36}Al_3Y$ (350.27): C 41.15, H 10.36; found: C 41.27, H 10.48.

Neodymium(III) tris(tetramethylaluminate) (1e): Following the procedure described above, $[NdCl_3(thf)_{1.75}]$ (5.47 g, 14.50 mmol), $LiNMe_2$ (2.22 g, 43.51 mmol), and $AlMe_3$ (8.36 g, 116.03 mmol) yielded **1e** as blue crystals (5.35 g, 13.20 mmol, 91%). ^1H NMR (500 MHz, $[D_6]$benzene, 25 °C): $\delta=10.53$ (brs, $\Delta\nu_{1/2}=40$ Hz, $Al(CH_3)_4$) ppm. ^{13}C NMR (151 MHz, $[D_6]$benzene, 25 °C): $\delta=281.5$ (brs, $\Delta\nu_{1/2}=180$ Hz, $Al(CH_3)_4$) ppm. ^{27}Al NMR (130 MHz, $[D_6]$benzene, 25 °C): $\delta=346$ (brs, $\Delta\nu_{1/2}=2874$ Hz, $Al(CH_3)_4$) ppm. IR (nujol): $\tilde{\nu}=1455$ (vs, nujol), 1378 (vs, nujol), 1306 (w), 1212 (vs), 1129 (w), 1052 (w), 975 (w), 925 (w), 892 (w), 859 (w), 726 (vs), 699 (vs), 561(vs), 541 cm^{-1} (vs). Elemental analysis (%) calcd for $C_{12}H_{36}Al_3Nd$ (405.60): C 35.54, H 8.95; found: C 35.27, H 8.70.

Samarium(III) tris(tetramethylaluminate) (1f): Following the procedure described above, $[SmCl_3(thf)_2]$ (5.48 g, 13.66 mmol), $LiNMe_2$ (2.09 g, 40.99 mmol), and $AlMe_3$ (7.88 g, 109.30 mmol) yielded **1f** as yellow crystals (4.52 g, 10.99 mmol, 80%). ^1H NMR (500 MHz, $[D_6]$benzene, 25 °C): $\delta=-3.06$ (brs, $\Delta\nu_{1/2}=10$ Hz, $Al(CH_3)_4$) ppm. ^1H NMR (500 MHz, $[D_8]$toluene, 25 °C): $\delta=-2.83$ (brs, $\Delta\nu_{1/2}=14$ Hz, $Al(CH_3)_4$) ppm. ^{13}C NMR (151 MHz, $[D_6]$benzene, 25 °C): $\delta=-31.5$ (brs, $\Delta\nu_{1/2}=54$ Hz, $Al(CH_3)_4$) ppm. ^{27}Al NMR (130 MHz, $[D_6]$benzene, 25 °C): $\delta=163$ (brs, $\Delta\nu_{1/2}=1836$ Hz , $Al(CH_3)_4$) ppm. IR (nujol): $\tilde{\nu}=1458$ (vs, nujol), 1380 (vs, nujol), 1303 (w), 1199 (vs), 966 (w), 940 (w), 919 (w), 852 (w), 723 (vs), 697 (vs), 572 (vs), 547 cm^{-1} (vs). Elemental analysis (%) calcd for $C_{12}H_{36}Al_3Sm$ (411.72): C 35.01, H 8.81; found: C 35.32, H 8.63.

Holmium(III) tris(tetramethylaluminate) (1g): Following the procedure described above, $[HoCl_3(thf)_{3.33}]$ (0.460 g, 0.90 mmol), $LiNMe_2$ (0.138 g, 2.70 mmol), and $AlMe_3$ (0.519 g, 7.20 mmol) yielded **1g** as pink crystals (0.307 g, 0.72 mmol, 80%). IR (nujol): $\tilde{\nu}=1458$ (vs, nujol), 1380 (vs, nujol), 1308 (w), 1220 (s), 1204 (w), 1090 (w), 966 (w), 899 (w), 847 (w), 728 (vs), 692 (vs), 562 cm^{-1} (vs). Elemental analysis (%) calcd for $C_{12}H_{36}Al_3Ho$ (426.29): C 33.81, H 8.51; found: C 33.67, H 8.48.

Lanthanum(III) tris(tetramethylaluminate) (1b): The synthesis of this complex has been reported previously.[17] ^1H NMR (500 MHz,

[D_8]toluene, 25 °C): $\delta = 0.05$ (s, Al(CH_3)$_4$) ppm. ^{27}Al NMR (130 MHz, [D_6]benzene, 25 °C): $\delta = 165$ (br s, $\Delta\nu_{1/2} = 1928$ Hz, *Al*(CH_3)$_4$) ppm.

Lutetium(III) tris(tetramethylaluminate) (1h): The synthesis of this complex has been reported previously.[6] ^{1}H NMR (500 MHz, [D_8]toluene, 25 °C): $\delta = 0.16$ (br s, $\Delta\nu_{1/2} = 72$ Hz, Al(CH_3)$_4$) ppm. ^{27}Al NMR (130 MHz, [D_6]benzene, 25 °C): $\delta = 163$ (br s, $\Delta\nu_{1/2} = 2262$ Hz, *Al*(CH_3)$_4$) ppm.

General procedure for the synthesis of lanthanide(III) tris(tetramethylaluminate)s 1c and 1d: THF (10 mL) was slowly added to a suspension of $LnCl_3$ in toluene (5 mL) at ambient temperature. $LiNMe_2$ was then slowly added as a solid and the mixture stirred at ambient temperature for 18 h. The solvent was removed in vacuo and the residue re-suspended in hexane (10 mL). $AlMe_3$ (7.5 equiv) was slowly added to this suspension and the mixture stirred for another 18 h at ambient temperature. It was then centrifuged and filtered through Celite to remove the insoluble LiCl. Solvent, excess $AlMe_3$, and the volatile by-product [{$Me_2Al(\mu$-$NMe_2)_2$}$_2$] were removed in vacuo and the residue was finally crystallized from hexane at −30 °C.

Cerium(III) tris(tetramethylaluminate) (1c): Following the procedure described above, $CeCl_3$ (1.48 g, 6.00 mmol), $LiNMe_2$ (0.92 g, 18.0 mmol), and $AlMe_3$ (3.26 g, 45.00 mmol) yielded **1c** as pale yellow crystals (1.18 g, 2.90 mmol, 74 %). IR (nujol): $\tilde{\nu} = 1458$ (vs, nujol), 1380 (vs, nujol), 1303 (w), 1196 (s), 1033 (m), 692 (s), 571 (s), 551 (s), 470 cm^{-1} (m). Elemental analysis (%) calcd for $C_{12}H_{36}Al_3Ce$ (401.84): C 35.90, H 9.04; found: C 35.90, H 9.31.

Praseodymium(III) tris(tetramethylaluminate) (1d): Following the procedure described above, $PrCl_3$ (0.99 g, 4.0 mmol), $LiNMe_2$ (0.61 g, 12.00 mmol), and $AlMe_3$ (2.16 g, 30.00 mmol) yielded **1d** as pale green crystals (1.184 g, 2.90 mmol, 74 %). ^{1}H NMR (500 MHz, [D_6]benzene, 25 °C): $\delta = 8.43$ (br s, $\Delta\nu_{1/2} = 22$ Hz, Al(CH_3)$_4$) ppm. ^{13}C NMR (126 MHz, [D_6]benzene, 25 °C): $\delta = 207.0$ (br s, $\Delta\nu_{1/2} = 56$ Hz, Al(CH_3)$_4$) ppm. ^{27}Al NMR (130 MHz, [D_6]benzene, 25 °C): $\delta = 317.4$ (br s, $\Delta\nu_{1/2} = 2876$ Hz, *Al*(CH_3)$_4$) ppm. IR (nujol): $\tilde{\nu} = 1458$ (vs, nujol), 1380 (vs, nujol), 1304 (w), 1197 (s), 1019 (w), 693 (s), 568 (s), 550 (s), 468 cm^{-1} (m). Elemental analysis (%) calcd for $C_{12}H_{36}Al_3Pr$ (402.28): C 35.83, H 9.02; found: C 35.91, H 9.45.

[Ce{($O_2CC_6H_2$*i*Pr_3-2,4,6)$_2$(μ-$AlMe_2$)}$_2$($AlMe_4$)(C_6H_{14})] (2c): Solid 2,4,6-triisopropyl benzoic acid (0.534 g, 2.15 mmol, 4.0 equiv) was slowly added to a well-stirred solution of **1c** (0.216 g, 0.54 mmol) in hexane (10 mL) at ambient temperature. After the evolution of methane had ceased the slightly yellow solution was stirred for a further hour at ambient temperature. The solvent was then reduced to about one half and the mixture was stored overnight at −30 °C. The mother liquid was separated from the pale yellow crystalline solid, which was washed with a small amount of cold hexane and finally dried in vacuo to give analytically pure **2c** (0.628 g, 0.44 mmol, 82 %). IR (nujol): $\tilde{\nu} = 1619$ (s), 1575 (w), 1528 (s), 1427 (s), 1365 (s), 1351 (s), 1332 (s), 1317 (s), 1197 (m), 1154 (m), 1109 (m), 1087 (w), 940 (w), 878 (m), 779 (m), 699 (s), 632 (m), 592 (w), 490 (w), 459 cm^{-1} (w). Elemental analysis (%) calcd for $C_{78}H_{130}Al_3CeO_8$ (1417.0): C 66.12, H 9.25; found: C 65.91, H 9.71.

[Pr{($O_2CC_6H_2$*i*Pr_3-2,4,6)$_2$(μ-$AlMe_2$)}$_2$($AlMe_4$)(C_6H_{14})] (2d): Following the procedure described above for **2c**, **1d** (0.205 g, 0.51 mmol), and 2,4,6-triisopropylbenzoic acid (0.506 g, 2.04 mmol, 4 equiv) gave **2d** as a pale green crystalline solid (0.620 g, 0.44 mmol, 86 %). IR (nujol): $\tilde{\nu} = 1621$ (s), 1575 (w), 1528 (s), 1351 (s), 1332 (s), 1317 (s), 1196 (m), 1154 (m), 1109 (m), 1087 (w), 940 (w), 878 (m), 779 (m), 699 (s), 631 (m), 591 (w), 490 (w), 458 cm^{-1} (w). Elemental analysis (%) calcd for $C_{78}H_{130}Al_3PrO_8$ (1417.7): C 66.08, H 9.24; found: C 66.27, H 9.67.

[Ce{OSi(O*t*Bu)$_3$}($AlMe_3$)($AlMe_4$)$_2$] (3c): Solid HOSi(O*t*Bu)$_3$ (0.158 g, 0.60 mmol, 1.0 equiv) was slowly added to a well-stirred solution of **1c** (0.239 g, 0.60 mmol) in hexane (7 mL) at ambient temperature. After the evolution of methane had ceased the bright yellow solution was stirred for a further hour at ambient temperature. The solvent was then removed in vacuo and the residue redissolved in hexane (3 mL). This solution was filtered through a pad of Celite and left to crystallize overnight at −30 °C. The mother liquid was then removed and the yellow crystalline solid washed with a small amount of cold hexane and dried in vacuo to give **3c** as a yellow crystalline solid (0.306 g, 0.47 mmol, 78 %). IR (nujol): $\tilde{\nu} = 1369$ (s), 1304 (w), 1246 (m), 1190 (s), 1090 (s), 1063 (s), 1028 (m), 945 (w), 922 (m), 899 (s), 832 (w), 822 (w), 803 (w), 705 (s), 604 (w), 574 (m), 530 (m), 489 (m), 436 cm^{-1} (w). Elemental analysis (%) calcd for $C_{23}H_{60}Al_3CeO_4Si$ (649.88): C 42.51, H 9.31; found: C 42.60, H 9.55.

[Pr{OSi(O*t*Bu)$_3$}($AlMe_3$)($AlMe_4$)$_2$] (3d): Following the procedure described above for **3c**, **1d** (0.196 g, 0.49 mmol), and HOSi(O*t*Bu)$_3$ (0.129 g, 0.49 mmol, 1 equiv) gave **3d** as a pale green crystalline solid (0.237 g, 0.36 mmol, 75 %). IR (nujol): $\tilde{\nu} = 1370$ (s), 1304 (w), 1245 (m), 1190 (s), 1171 (m), 1091 (s), 1062 (s), 1028 (m), 948 (w), 922 (m), 897 (s), 832 (w), 822 (w), 803 (w), 692 (s), 602 (w), 574 (m), 528 (m), 488 (m), 435 cm^{-1} (w). Elemental analysis (%) calcd for $C_{23}H_{60}Al_3PrO_4Si$ (650.67): C 42.46, H 9.29; found: C 42.58, H 9.49.

Polymerization of isoprene: All manipulations were performed in a glove box under argon. A detailed polymerization procedure (run 10 of Table 7) is described here as a typical example. Et_2AlCl (2.5 μL, 0.02 mmol, 1 equiv) was added to a solution of **2c** (27.7 mg, 0.02 mmol) in hexane (8 mL) and the mixture was "aged" for 30 min. The polymerization was carried out at 40 °C for 24 h after addition of isoprene (2.0 mL, 20 mmol). The polymerization mixture was then poured into a large quantity of acidified isopropanol containing 0.1 % (w/w) 2,6-di-*tert*-butyl-4-methylphenol as a stabilizer. The polymer was washed with isopropanol and dried in vacuo at ambient temperature to constant weight. The monomer conversion was determined gravimetrically.

Polymer analyses: The molar masses (M_w, M_n) of the polymers were determined by size-exclusion chromatography (SEC) with an SEC apparatus fitted with a pump supplied by Waters (Waters 510) and Ultrastyragel columns with pore sizes of 500, 1000, 10000, and 100000 Å (eluent: $CHCl_3$; flow rate: 0.5 mL min^{-1}). Sample solutions (1.0 mg of polymer per milliliter of $CHCl_3$) were filtered through a 0.2 μm syringe filter prior to injection. The signals were detected with a differential refractometer (Waters 410) and calibrated against polystyrene standards from Fluka ($M_w/M_n < 1.15$). The microstructure of polyisoprenes was examined by ^{13}C NMR spectroscopy in $CDCl_3$.

NMR spectroscopy

Sample preparation: [Ln($AlMe_4$)$_3$] was dissolved in [D_8]toluene for the low temperature studies, in [D_5]chlorobenzene for the high temperature studies, and in [D_6]benzene for multinuclear studies at ambient temperature with a concentration of approximately 0.25 M.

High-resolution NMR spectra were acquired with Bruker Biospin AV500 and AV600 spectrometers equipped with narrow-bore UltraShieldPlus magnets. A 5-mm broadband probe head equipped with a z-gradient coil was used on the AV500. The temperature was set and stabilized with a Bruker B-VT 3000 temperature controller unit regulating the boil-off rate of liquid nitrogen for the variable temperature experiments or the heating of the gas flow from a BCU5 cooling unit for the other NMR experiments. A 5-mm triple resonance (^{1}H, ^{13}C, ^{15}N) inverse CryoProbe was used on the AV600. Only ^{1}H (600.13 MHz) and broadband ^{1}H-decoupled ^{13}C (150.91 MHz) spectra at 298 K were recorded on the AV600. Variable-temperature ^{1}H (500.13 MHz) and broadband ^{1}H-decoupled ^{13}C (125.77 MHz) spectra were acquired on the AV500. The temperature scales on both spectrometers were calibrated against a standard sample (Bruker) containing 4 % methanol in [D_4]methanol. The average estimated uncertainty of the real temperature inside the NMR tubes was 1 K. The sample temperatures were kept at 298 K for all other than the variable-temperature experiments. The ^{89}Y NMR spectra of [Y($AlMe_4$)$_3$] dissolved in [D_8]toluene were acquired at 24.51 MHz on the AV500. For the 1D ^{89}Y experiment, the pulse width was 9 μs (approx. 55° flip angle), the recycling delay 30 s, and 176 scans were averaged. ^{1}H inverse-gated decoupling was used to minimize any possible intensity loss from negative NOE effects on ^{89}Y. The total experimental time for the ^{89}Y NMR experiment was 2 h 20 min. A two-dimensional ^{1}H-detected ^{1}H-^{89}Y HMQC[60,61] spectrum was acquired in the pure-absorption mode. Since ^{89}Y is present at 100 % natural abundance, no gradients were required for coherence selection. A total of 32 t_1 increments were collected. Four transients were averaged for each increment and the recycling delay was 2 s. The experiment was optimized for $^2J_{H,Y} = 2.5$ Hz. Broadband ^{89}Y decoupling (composite pulse decoupling) was used during the acquisition. The total experimental time was 7 min. ^{27}Al spectra of [Ln($AlMe_4$)$_3$] were recorded on the AV500 at 130.33 MHz. 2000 scans were averaged. The

NMR spectroscopic data were processed and displayed using iNMR[62] and Bruker's TopSpin software. The residual ^{1}H signal of the deuterated solvents and ^{13}C solvent signals were used as secondary chemical shift references, and the chemical shifts are thus referenced to internal solvent resonances and reported in parts per million relative to TMS. The Ξ-scale was used to reference the ^{89}Y chemical shift.[63] Thus, Ξ = 4.900198 MHz for ^{89}Y and the measured absolute frequency at δ = 0.00 ppm for ^{1}H when using the secondary reference, gives a reference frequency for the ^{89}Y chemical shifts. The ^{27}Al chemical shifts are reported relative to an external reference, namely a solution of $AlCl_3$ in D_2O with a drop of concentrated HCl [$Al(D_2O)_6^{3+}$].

The MEXICO program[34] was used to analyze the variable temperature ^{1}H and ^{13}C NMR spectra by line-shape analyses of the methyl regions of the spectra. The spectral regions were fitted to a mutual two-site exchange model (equal populations) using a simplex-based iterative procedure. The MEXICO program takes into account the (slight) variations of the ^{1}H and ^{13}C chemical shifts with temperature and the heteronuclear $^2J_{Y,H}$ and $^1J_{Y,C}$ couplings. Based on variations seen in the rate constants upon adjusting some model parameters, and the quality of the fits (based on χ^2), the average uncertainties for the rate constants are estimated at 10% and 20% for the ^{1}H and ^{13}C spectral series, respectively. The varying contribution from inhomogeneities and the natural linewidths, as well as the limited spectral signal-to-noise ratios, especially for the ^{13}C spectra, all contribute to the uncertainties. The QtiPlot program was used to plot, fit, and extract the activation parameters from the kinetic data.[64] A linear least-squares fitting procedure was used to calculate the activation parameters from the Eyring equation. The uncertainties in the activation parameters were calculated with error propagation formulae.[65,66] In addition, a comparison was made with results from nonlinear fitting schemes (with and without weighting of the data points). This comparison revealed moderate deviations between the values obtained from the various fitting schemes, and also suggested that the uncertainties found using the error propagation formulas were reasonable.

Single-crystal X-ray structures

Crystal data and details of the structure determination are presented in Table 8.

*Compounds **1d**, **1h**, and **3d***: A suitable single crystal was transferred into a Lindemann capillary, fixed, and sealed. Data collection was carried out on an area detecting system (Nonius, MACH3, κ-CCD) at the window of a rotating anode (Nonius, FR591) with graphite monochromated $Mo_{K\alpha}$ radiation (λ = 0.71073 Å) at 173, 123, and 153 K, respectively (Oxford Cryosystems). Nine data sets were measured in rotation scan modus with $\Delta\phi/\Delta\omega$ = 1.0°. The structure was solved using SIR92 and full-matrix least-squares refinement made with SHELXL-97.[67] All hydrogen positions were refined with individual isotropic displacement parameters for **1h**. Noncoordinating methyl groups in **1d** and **3d** were refined as rigid and rotating (difference Fourier density optimization) CH_3 groups around the respective C–Al bonds. Coordinating methyl groups were refined as rigid pyramidal groups with the same C–H and H–H distances as for the previous, but with the threefold axis of the pyramidal rigid group allowed to be nonparallel to the C–Al bond axis. The isotropic displacement parameters for all H atoms were set to be 1.5 times that of the pivot C atom.

*Compounds **1b** and **1f***: The crystals were placed in a nylon loop containing Paratone oil (Hampton Research) and mounted directly into the N_2 cold stream (Oxford Cryosystems Series 600) on a Bruker AXS SMART 2 K CCD diffractometer. Data were collected by means of 0.3°ω-scans in four orthogonal φ-settings using $Mo_{K\alpha}$ radiation (λ = 0.71073 Å). Data collection was controlled by the program SMART, data integration by SAINT, and structure solution and model refinement were performed with SHELXS-97[68b] and SHELXL-97,[67f] respectively. Noncoordinating

Table 8. Crystallographic data for compounds **1b**, **1d**, **1f**, **1h**, and **3d**.

	1b	**1d**	**1f**	**1h**	**3d**
formula	$C_{12}H_{36}Al_3La$	$C_{12}H_{36}Al_3Pr$	$C_{12}H_{36}Al_3Sm$	$C_{12}H_{36}Al_3Lu$	$C_{23}H_{60}Al_3O_4PrSi$
Fw	400.26	402.26	411.723	436.32	650.65
color/habit	colorless/prism	pale green/needle	yellow/needle	colorless/fragment	pale green/plate
crystal dimensions [mm^3]	0.40×0.38×0.30	0.62×0.30×0.21	0.57×0.22×0.12	0.25×0.30×0.58	0.33×0.31×0.31
cryst system	monoclinic	monoclinic	monoclinic	monoclinic	monoclinic
space group	$P2_1/n$	$P2_1/c$	$C2/c$	$C2/c$	$P2_1/c$
a [Å]	15.4744(14)	7.4567(1)	10.8844(4)	10.8848(1)	10.2408(1)
b [Å]	7.3837(7)	17.9165(1)	15.9478(6)	15.6948(1)	17.2826(2)
c [Å]	17.5984(16)	32.5452(2)	12.6732(5)	12.4838(1)	20.0699(2)
β [°]	91.753(2)	92.0119(2)	102.932(1)	101.8067(3)	104.7609(6)
V [Å^3]	2009.8(3)	4345.29(7)	2144.05(14)	2087.55(3)	3434.90(6)
Z	4	8	4	4	4
T [K]	123(2)	173(2)	123(2)	123(1)	153(2)
ρ_{calcd} [mg m^{-3}]	1.323	1.230	1.275	1.388	1.258
μ [mm^{-1}]	2.238	2.347	2.845	4.838	1.552
F(000)	816	1648	836	872	1368
θ range [°]	1.73/30.11	2.20/26.27	2.31/30.08	2.31/25.29	2.10/26.38
index ranges	$-21\le h\le 21$, $-10\le k\le 10$, $-24\le l\le 24$	$-9\le h\le 9$, $-22\le k\le 21$, $-40\le l\le 39$	$-15\le h\le 15$, $-22\le k\le 22$, $-17\le l\le 17$	$-13\le h\le 13$, $-18\le k\le 18$, $-14\le l\le 14$	$-12\le h\le 12$, $-21\le k\le 21$, $-25\le l\le 23$
no. of rflns collected	33491	45964	18226	25693	84999
no. of indep rflns/R_{int}	5902/0.0261	8676/0.0415	3146/0.0163	1901/0.040	6887/0.0657
No. of obsd rflns ($I>2\sigma(I)$)	5626	7696	3088	1892	5486
data/restraints/params	5902/48/221	8676/72/409	3146/18/104	1901/0/147	6887/30/365
$R1$/$wR2$ ($I>2\sigma(I)$)[a]	0.0275/0.0743	0.0225/0.0448	0.0103/0.0276	0.0102/0.0248	0.0314/0.0576
$R1$/$wR2$ (all data)[a]	0.0287/0.0747	0.0287/0.0466	0.0107/0.0278	0.0103/0.0248	0.0503/0.0624
GOF (on F^2)[a]	1.284	1.077	1.110	1.113	1.054
largest diff peak and hole [e Å^{-3}]	1.464/−0.867	0.409/−0.423	0.274/−0.662	0.46/−0.50	1.100/−0.602

[a] $R1=\Sigma(||F_0|-|F_c||)/\Sigma|F_0|$; $wR2=\{\Sigma[w(F_0^2-F_c^2)^2]/\Sigma[w(F_0^2)^2]\}^{1/2}$; GOF = $\{\Sigma[w(F_0^2-F_c^2)^2]/(n-)\}^{1/2}$.

methyl groups were refined as rigid and rotating (difference Fourier density optimization) CH_3 groups around the respective C–Al bonds. Coordinating methyl groups were refined as rigid pyramidal groups with the same C–H and H–H distances as for the previous, but with the threefold axis of the pyramidal rigid group allowed to be nonparallel to the C–Al bond axis. The isotropic displacement parameters for all H atoms were set to be 1.5 times that of the pivot C atom.

CCDC-642735–CCDC-642739 contain the supplementary crystallographic data for this paper. These data can be obtained free of charge from the Cambridge Crystallographic Data Center via www.ccdc.cam.ac.uk/data_request/cif.

Acknowledgments

Financial support from the Norwegian Research Council (project no. 171245V30) and the program Nanoscience@UiB is gratefully acknowledged. We also thank Dr. L. Friebe (c/o Prof. O. Nuyken) for GPC analysis and Rannveig Litlabø for providing a sample of $[Pr(AlMe_4)_3]$.

[1] a) J. M. Birmingham, G. Wilkinson, *J. Am. Chem. Soc.* **1954**, *76*, 6210; b) J. M. Birmingham, G. Wilkinson, *J. Am. Chem. Soc.* **1956**, *78*, 42.
[2] H. Gilman, R. G. Jones, *J. Am. Chem. Soc.* **1945**, *67*, 505.
[3] F. A. Hart, A. G. Massey, M. S. Saran, *J. Organomet. Chem.* **1970**, *21*, 147.
[4] Reviews: a) F. T. Edelmann, *Top. Curr. Chem.* **1996**, *179*, 247; b) H. Yasuda, *Top. Organomet. Chem.* **1999**, *2*, 255; c) R. Anwander in *Applied Homogeneous Catalysis with Organometallic Compounds* (Eds.: B. Cornils, W. A. Herrmann), Wiley-VCH, Weinheim, **2002**, p. 974; d) F. T. Edelmann, D. M. M. Freckmann, H. Schumann, *Chem. Rev.* **2002**, *102*, 1851.
[5] a) G. K. Barker, M. F. Lappert, *J. Organomet. Chem.* **1974**, *76*, C45; b) P. B. Hitchcock, M. F. Lappert, R. G. Smith, R. A. Bartlett, P. P. Power, *J. Chem. Soc. Chem. Commun.* **1988**, 1007.
[6] H. M. Dietrich, G. Raudaschl-Sieber, R. Anwander, *Angew. Chem.* **2005**, *117*, 5437; *Angew. Chem. Int. Ed.* **2005**, *44*, 5303.
[7] a) H. Schumann, J. Müller, *Angew. Chem.* **1978**, *90*, 307; *Angew. Chem. Int. Ed. Engl.* **1978**, *17*, 276; b) H. Schumann, J. Pickardt, N. Bruncks, *Angew. Chem.* **1981**, *93*, 127; *Angew. Chem. Int. Ed. Engl.* **1981**, *20*, 120; c) H. Schumann, J. Müller, N. Bruncks, H. Lauke, J. Pickardt, H. Schwarz, K. Eckart, *Organometallics* **1984**, *3*, 69; d) H. Schumann, H. Lauke, E. Hahn, J. Pickardt, *J. Organomet. Chem.* **1984**, *263*, 29; e) A. L. Wayda, W. J. Evans, *J. Am. Chem. Soc.* **1978**, *100*, 7119; f) J. L. Atwood, M. F. Lappert, H. Zhang, *J. Chem. Soc. Chem. Commun.* **1988**, 1308.
[8] a) M. F. Lappert, R. Pearce, *J. Chem. Soc. Chem. Commun.* **1973**, 126; b) J. L. Atwood, W. E. Hunter, R. D. Rogers, J. Holton, J. McMeeking, R. Pearce, M. F. Lappert, *J. Chem. Soc. Chem. Commun.* **1978**, 140; c) H. Schumann, J. Müller, *J. Organomet. Chem.* **1978**, *146*, C5; d) H. Schumann, D. M. M. Freckmann, S. Dechert, *Z. Anorg. Allg. Chem.* **2002**, *628*, 2422; e) M. Niemeyer, *Acta Crystallogr. Sect. A* **2001**, *E57*, m553; f) W. J. Evans, J. C. Brady, J. W. Ziller, *J. Am. Chem. Soc.* **2001**, *123*, 7711.
[9] D. J. H. Emslie, W. E. Piers, M. Parvez, R. McDonald, *Organometallics* **2002**, *21*, 4226.
[10] M. Niemeyer, *Z. Anorg. Allg. Chem.* **2000**, *626*, 1027.
[11] S. Bambirra, A. Meetsma, B. Hessen, *Organometallics* **2006**, *25*, 3454.
[12] H. H. Karsch, A. Appelt, G. Müller, *Angew. Chem.* **1986**, *98*, 832; *Angew. Chem. Int. Ed. Engl.* **1986**, *25*, 823.
[13] a) M. Booij, N. H. Kiers, H. J. Heeres, J. H. Teuben, *J. Organomet. Chem.* **1989**, *364*, 79; b) A. L. Wayda, R. D. Rogers, *Organometallics* **1985**, *4*, 1440; c) L. E. Manzer, *J. Am. Chem. Soc.* **1978**, *100*, 8068; d) S. Harder, *Organometallics* **2005**, *24*, 373.
[14] a) W. J. Evans, R. Anwander, J. W. Ziller, *Organometallics* **1995**, *14*, 1107; b) W. T. Klooster, R. S. Lu, R. Anwander, W. J. Evans, T. E. Koetzle, R. Bau, *Angew. Chem.* **1998**, *110*, 1326; *Angew. Chem. Int. Ed.* **1998**, *37*, 1268.
[15] A. Fischbach, R. Anwander, *Adv. Polym. Sci.* **2006**, *204*, 155.
[16] A. Fischbach, F. Perdih, E. Herdtweck, R. Anwander, *Organometallics* **2006**, *25*, 1626.
[17] A. Fischbach, M. G. Klimpel, M. Widenmeyer, E. Herdtweck, W. Scherer, R. Anwander, *Angew. Chem.* **2004**, *116*, 2284; *Angew. Chem. Int. Ed.* **2004**, *43*, 2234.
[18] H. M. Dietrich, C. Zapilko, E. Herdtweck, R. Anwander, *Organometallics* **2005**, *24*, 5767.
[19] H. M. Dietrich, M. Zimmermann, R. Anwander, unpublished results.
[20] M. Zimmermann, K. W. Törnroos, R. Anwander, *Organometallics* **2006**, *25*, 3593.
[21] M. Zimmermann, K. W. Törnroos, R. Anwander, *Angew. Chem.* **2007**, *119*, 3187; *Angew. Chem. Int. Ed. Engl.* **2007**, *46*, 3126.
[22] E. Le Roux, F. Jaroschik, F. Nief, K. W. Törnroos, R. Anwander, unpublished results.
[23] H. M. Dietrich, K. W. Törnroos, R. Anwander, *J. Am. Chem. Soc.* **2006**, *128*, 9298.
[24] H. M. Dietrich, H. Grove, K. W. Törnroos, R. Anwander, *J. Am. Chem. Soc.* **2006**, *128*, 1458.
[25] Due to the low solubilities of the trichlorides of the larger lanthanide metals, Soxhlet extraction with thf to generate the activated $[LnCl_3(thf)_x]$ complexes is time consuming.
[26] R. Anwander, O. Runte, J. Eppinger, G. Gerstberger, E. Herdtweck, M. Spiegler, *J. Chem. Soc. Dalton Trans.* **1998**, 847.
[27] D. M. Barnhart, D. L. Clark, J. C. Gordon, J. C. Huffman, J. G. Watkin, B. D. Zwick, *J. Am. Chem. Soc.* **1993**, *115*, 8461.
[28] R. Anwander, M. G. Klimpel, H. M. Dietrich, D. J. Shorokhov, W. Scherer, *Chem. Commun.* **2003**, 1008.
[29] W. J. Evans, L. R. Chamberlain, T. A. Ulibarri, J. W. Ziller, *J. Am. Chem. Soc.* **1988**, *110*, 6423.
[30] G. R. Patzke, R. Wartchow, W. Urland, *Z. Anorg. Allg. Chem.* **2000**, *626*, 789.
[31] H. M. Dietrich, O. Schuster, K. W. Törnroos, R. Anwander, *Angew. Chem.* **2006**, *118*, 4977; *Angew. Chem. Int. Ed.* **2006**, *45*, 4858.
[32] M. E. O'Neill, K. Wade in *Comprehensive Organometallic Chemistry* (Eds.: G. Wilkinson, F. G. A. Stone, E. W. Abel), Pergamon Press, New York, **1982**, p. 593.
[33] J. Eppinger, *PhD Thesis*, **1999**, Technische Universität München.
[34] a) A. D. Bain, G. J. Duns, *Can. J. Chem.* **1996**, *74*, 819; b) A. D. Bain, D. M. Rex, R. N. Smith, *Magn. Reson. Chem.* **2001**, *39*, 122.
[35] W. von Philipsborn, *Chem. Soc. Rev.* **1999**, *28*, 95.
[36] P. G. Plieger, K. D. John, T. S. Keizer, T. M. McCleskey, A. K. Burell, R. L. Martin, *J. Am. Chem. Soc.* **2004**, *126*, 14651.
[37] P. J. Shapiro, *Coord. Chem. Rev.* **1999**, *189*, 1.
[38] C. J. Schaverien, *Organometallics* **1994**, *13*, 69.
[39] W. J. Evans, J. H. Meadows, A. G. Kostka, G. L. Closs, *Organometallics* **1985**, *4*, 324.
[40] R. E. White, T. P. Hanusa, *Organometallics* **2006**, *25*, 5621.
[41] S. Arndt, J. Okuda, *Adv. Synth. Catal.* **2005**, *347*, 339.
[42] M. G. Klimpel, R. Anwander, M. Tafipolsky, W. Scherer, *Organometallics* **2001**, *20*, 3983.
[43] R. Benn, E. Janssen, H. Lehmkuhl, A. Rufinska, K. Angermund, P. Betz, R. Goddard, C. Krüger, *J. Organomet. Chem.* **1991**, *411*, 37.
[44] H. E. Swift, C. P. Pole, J. F. Itzel, *J. Phys. Chem.* **1964**, *68*, 2509.
[45] D. E. O'Reilly, *J. Chem. Phys.* **1960**, *32*, 1007.
[46] B. W. Epperlein, O. Lutz, *Z. Naturforsch. A* **1968**, *23*, 1413.
[47] J. W. Akitt, *Annu. Rep. NMR Spectrosc.* **1972**, *5A*, 465.
[48] A. Fischbach, F. Perdih, P. Sirsch, W. Scherer, R. Anwander, *Organometallics* **2002**, *21*, 4569.
[49] A. Fischbach, G. Eickerling, W. Scherer, E. Herdtweck, R. Anwander, *Z. Naturforsch. B* **2004**, *59*, 1353.
[50] R. Anwander, *Chem. Mater.* **2001**, *13*, 4419.
[51] Z. Shen, J. Ouyang, F. Wang, Z. Hu, Y. Fu, B. Qian, *J. Polym. Sci.: Polym. Chem. Ed.* **1980**, *18*, 3345.

[52] Y. B. Monakov, N. G. Marina, I. G. Savel'eva, L. E. Zhiber, V. G. Kozlov, S. R. Rafikov, *Dokl. Akad. Nauk SSSR* **1982**, *265*, 1431; *Chem. Abstr.* **1983**, *98*, 54523.
[53] J. Witte, *Angew. Makromol. Chem.* **1981**, *94*, 119.
[54] L. Friebe, O. Nuyken, H. Windisch, W. Obrecht, *Macromol. Chem. Phys.* **2002**, *203*, 1055.
[55] A. Pross, P. Marquardt, K. H. Reichert, W. Nentwig, T. Knauf, *Angew. Makromol. Chem.* **1997**, *249*, 59.
[56] L. Friebe, O. Nuyken, W. Obrecht, *J. Macromol. Sci. Pure Appl. Chem.* **2005**, *42*, 839.
[57] C. Boisson, F. Barbotin, R. Spitz, *Macromol. Chem. Phys.* **1999**, *200*, 1163.
[58] J. Yamamoto, C. A. Wilkie, *Inorg. Chem.* **1971**, *10*, 1129.
[59] H. Tani, T. Konomi, *J. Polym. Sci., Part A* **1966**, *4*, 301.
[60] L. Müller, *J. Am. Chem. Soc.* **1979**, *101*, 4481.
[61] A. Bax, R. H. Griffey, B. L. Hawkins, *J. Magn. Reson.* **1983**, *55*, 301.
[62] Nucleomatica, http://www.inmr.net/index.html
[63] R. K. Harris, E. D. Becker, S. M. Cabral de Menezes, R. Goodfellow, P. Granger, *Pure Appl. Chem.* **2001**, *73*, 1795.
[64] http://soft.proindependent.com/qtiplot.html
[65] P. M. Morse, M. D. Spencer, S. R. Wilson, G. S. Girolami, *Organometallics* **1994**, *13*, 1646.
[66] Q. D. Shelby, W. Lin, G. S. Girolami, *Organometallics* **1999**, *18*, 1904.
[67] a) Data Software for NONIUS Collection κ-CCD devices, Delft (The Netherlands) **1997**; b) Z. Otwinowski, W. Minor, *Methods Enzymol.* **1997**, *276*, 307; c) *International Tables for Crystallography*, (Eds.: T. Hahn, A. J. C. Wilson), Kluwer Academic Publisher, Dordrecht, Boston, London, **1992**; d) A. L. Spek, PLATON: A Multipurpose Crystallographic Tool, Utrecht University, Utrecht (The Netherlands) **2007**; e) SIR92: A. Altomare, G. Cascarano, C. Giacovazzo, A. Guagliardi, M. C. Burla, G. Polidori, M. Camalli, *J. Appl. Cryst.* **1994**, *27*, 435; f) G. M. Sheldrick, SHELXL-97, University of Göttingen, Germany, **1998**.
[68] a) SMART, Ver. 5.054, **1999** and SAINT, Ver. 6.45a, Bruker AXS Inc., Madison, Wisconsin (USA), **2001**; b) G. M. Sheldrick, SHELXS-97, University of Göttingen, Germany, **2003**.

Received: April 4, 2007
Published online: July 24, 2007

